













Spatiotemporal control of miR398 biogenesis, via chromatin remodeling and kinase signaling, ensures proper ovule development

Hanyang Cai ¹, Liping Liu ¹, Man Zhang ¹, Mengnan Chai ¹, Youmei Huang ¹, Fangqian Chen ¹, Maokai Yan ², Zhenxia Su ¹, Ian Henderson ³, Ravishankar Palanivelu ⁴, Xuemei Chen ⁵, and Yuan Qin ^{1,2,*}

- 1 College of Life Science, Fujian Provincial Key Laboratory of Haixia Applied Plant Systems Biology, State Key Laboratory of Ecological Pest Control for Fujian and Taiwan Crops, Fujian Agriculture and Forestry University, Fuzhou 350002, China
- 2 State Key Laboratory for Conservation and Utilization of Subtropical Agro-Bioresources, Guangxi Key Lab of Sugarcane Biology, College of Agriculture, Guangxi University, Nanning 530004, China
- 3 Department of Plant Sciences, University of Cambridge, Downing Street, Cambridge CB2 3EA, United Kingdom
- 4 School of Plant Sciences, University of Arizona, Tucson, AZ 85721, United States
- 5 Department of Botany and Plant Sciences, Institute of Integrative Genome Biology, University of California, Riverside, CA 92521, United States

*Author for correspondence: yuanqin@fafu.edu.cn

H.C. cloned the genes; generated the transgenic lines; and performed phenotypic, expression, and genetic analyses. L.L. performed expression and genetic analyses. M.Z., M.C., F.C., M.Y., and Z.S. were involved in the phenotypic and genetic analyses. X.C., R.P., and I.H. interpreted the data and revised the manuscript. Y.Q. and H.C. designed the research and wrote the manuscript.

The author responsible for distribution of materials integral to the findings presented in this article in accordance with the policy described in the Instructions for Authors (<https://academic.oup.com/plcell>) is: Yuan Qin (yuanqin@fafu.edu.cn).

Abstract

The coordinated development of sporophytic and gametophytic tissues is essential for proper ovule patterning and fertility. However, the mechanisms regulating their integrated development remain poorly understood. Here, we report that the Swi2/Snf2-Related1 (SWR1) chromatin-remodeling complex acts with the ERECTA receptor kinase-signaling pathway to control female gametophyte and integument growth in *Arabidopsis thaliana* by inhibiting transcription of the microRNA gene *MIR398c* in early-stage megagametogenesis. Moreover, pri-miR398c is transcribed in the female gametophyte but is then translocated to and processed in the ovule sporophytic tissues. Together, SWR1 and ERECTA also activate *ARGONAUTE10* (*AGO10*) expression in the chalaza; *AGO10* sequesters miR398, thereby ensuring the expression of three *AGAMOUS-LIKE* (*AGL*) genes (*AGL51*, *AGL52*, and *AGL78*) in the female gametophyte. In the context of sexual organ morphogenesis, these findings suggest that the spatiotemporal control of miRNA biogenesis, resulting from coordination between chromatin remodeling and cell signaling, is essential for proper ovule development in *Arabidopsis*.

Introduction

Development in multicellular organisms requires coordinated growth and morphogenesis between tissues. In

Arabidopsis thaliana, ovules comprise the haploid female gametophyte (also called the embryo sac) and the surrounding diploid sporophytic tissues. Development of these distinct tissues must be integrated for proper ovule morphogenesis

and successful fertilization (Bencivenga et al., 2011; Chevalier et al., 2011). The Arabidopsis ovule primordium originates from the placenta, elongates along the proximal/distal axis, and develops into three regions; the nucellus, chalaza, and funiculus. The female germline initiates in the distal nucellus, followed by development of the female gametophyte. The proximal chalaza and funiculus differentiate into the integuments and stalk, respectively (Figure 1A). Arabidopsis ovules contain inner and outer integuments, each composed of two cell layers (Coen et al., 2017). The integuments envelop the female gametophyte while leaving a small opening known as a micropyle, through which pollen tubes enter to deliver sperm to the female gametophyte.

The development of the haploid female gametophyte is regulated by genes expressed in the female gametophyte and/or the surrounding ovule integuments (Yang and Sundaresan, 2000; Yadegari and Drews, 2004). Integument-expressed proteins that are important for the development of the female gametophyte include transcription factors (TFs) such as BELL1 (a homeodomain TF; Reiser et al., 1995), INNER NO OUTER (INO, a YABBY TF; Villanueva et al., 1999), and AINTEGUMENTA (ANT, an AP2 TF; Elliott et al., 1996; Klucher et al., 1996), and kinases such as TOUSLED (a nuclear Ser/Thr protein kinase; Roe et al., 1997), ERECTA (ER), ERECTA-LIKE 1 (ERL1), and ERL2 (leucine-rich repeat receptor-like kinases; Pillitteri et al., 2007), and MPK3 and MPK6 (mitogen-activated protein kinases, MPKs; Wang et al., 2008). Plant hormone signaling in the integuments also regulates female gametophyte development, including auxin (Pagnussat et al., 2009; Lituiev et al., 2013) and cytokinin (Kinoshita-Tsujimura and Kakimoto, 2011; Bencivenga et al., 2012; Cheng et al., 2013). Mutations in integument-expressed genes can cause defective integument elongation along with arrested female gametophyte development (Baker et al., 1997). Although many mutations in female gametophyte-expressed genes do not lead to obvious sporophytic integument growth defects (Colombo et al., 2008; Rabiger and Drews, 2013), altered integument gene expression has been detected in ovule mutants that lack a female gametophyte (Johnston et al., 2007; Armenta-Medina et al., 2013; Zhao et al., 2014). These reports suggest that the gametophyte and integument communicate and mutually influence each other's development.

Epigenetic regulatory pathways likely contribute to the coordinated development of the integument and female gametophytic tissues in the ovule. For example, a mutation in the SET DOMAIN GROUP2 (SDG2) gene, which mediates histone H3 lysine 4 trimethylation (H3K4me3), causes defective female gametophyte formation and inhibits integument growth (Berr et al., 2010). The ATP-dependent CHD3 chromatin remodeler PICKLE (PKL), which can be either positively or negatively associated with H3K27me3 in genes important for seed germination, was also reported to control female gametophyte development and integument growth (Carter et al., 2016). Several microRNAs (miRNAs), including miR167 and miR165/6, regulate ovule

morphogenesis and fertility by restricting the expression of their target genes AUXIN RESPONSE FACTORS ARF6 and ARF8 and the Class III homeodomain leucine zipper (HD-Zip III) gene PHABULOSA (PHB), respectively (Wu et al., 2006; Hashimoto et al., 2018). However, how these factors mediate the integrated development of the ovule integument and the female gametophyte is not well understood.

The ATP-dependent chromatin-remodeling complex SWR1 (SWI2/SNF2-Related 1) plays a crucial role in regulating gene expression by exchanging histone H2A-H2B dimers with H2A.Z-H2B dimers (Aslam et al., 2019). The H2A.Z histone variant is highly conserved throughout eukaryotes (van Daal et al., 1990). H2A.Z deposition into nucleosomes plays roles in fine-tuning gene expression, both positively and negatively, by changing chromatin architecture and transcription factor accessibility (Marques et al., 2010; Dai et al., 2017). In Arabidopsis, various SWR1 complex subunits such as PHOTOPERIOD INDEPENDENT EARLY FLOWERING1 (PIE1), ACTIN-RELATED PROTEIN6 (ARP6), SERRATED LEAVES AND EARLY FLOWERING (SEF), SWR1 COMPLEX SUBUNIT2 (SWC2), SWC4, and METHYL-CpG-BINDING DOMAIN9 (MBD9) have been identified (Lazaro et al., 2008; March-Diaz and Reyes, 2009; Potok et al., 2019; Sijacic et al., 2019; Luo et al., 2020). SWR1 orchestrates numerous aspects of growth and development, including leaf shape, organ size, flowering time, meiosis, and germline specification (Choi et al., 2005; Deal et al., 2005; Choi et al., 2007; Deal et al., 2007; Lazaro et al., 2008; March-Diaz and Reyes, 2009; Choi et al., 2013; Rosa et al., 2013; Zhao et al., 2018). Mutations in SWR1 complex subunit genes cause similar pleiotropic developmental phenotypes, although *pie1* mutants exhibit more severe phenotypes than *arp6* and *sef* (Mizuguchi et al., 2004).

Using genetic enhancer screening, we found that SWR1 genetically interacts with the ER-MPK-signaling pathway in the control of Arabidopsis ovule development. Specifically, they regulate the coordinated growth and development of the female gametophyte and integument by repressing the expression of *MIR398c* during early-stage megagametogenesis. We further show that SWR1 and ER-MPK signaling are critical for spatially inhibiting miR398 accumulation in the developing female gametophyte. miR398 would otherwise inhibit three target *AGAMOUS-LIKE* (AGL) genes (*AGL51*, *AGL52*, and *AGL78*) and disturb their function in female gametophyte development and integument growth. We also identified two mechanisms that prevent miR398 accumulation in the female gametophyte: 1) pri-miR398c is generated in the female gametophyte but is translocated to and processed in the ovule sporophytic tissues and 2) AGO10 plays a key role in sequestering miR398 in the chalaza. Our results indicate that chromatin remodeling is coordinated with a kinase-signaling pathway to ensure integrated development between sporophytic and gametophytic tissues, via precise spatial and temporal control of miR398 biogenesis. These findings provide new insights into sexual organ morphogenesis in higher plants.

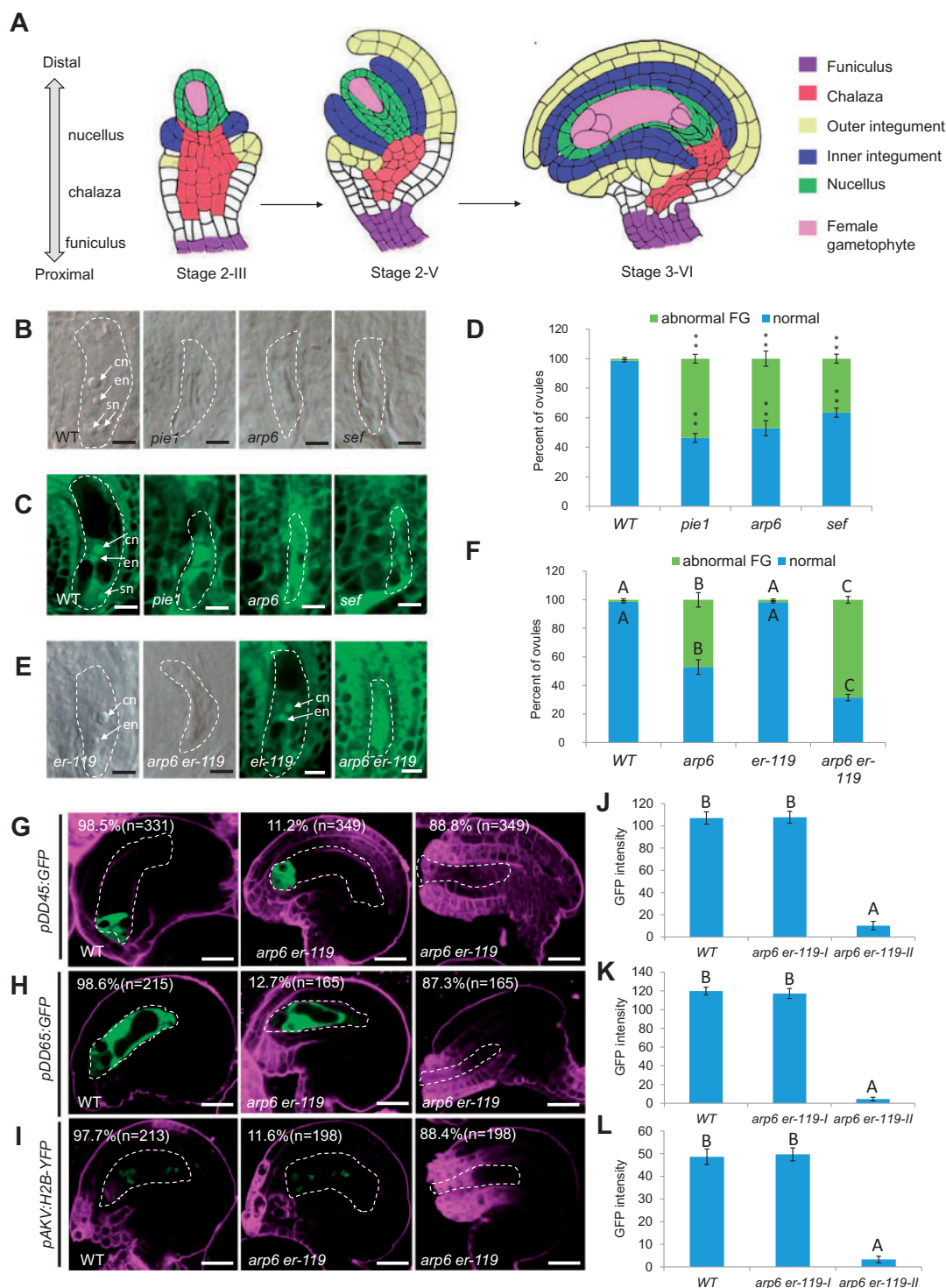


Figure 1 The *er-119* mutation enhanced the female gametophyte developmental defects in SWR1 complex mutant. **A**, Diagram illustrating the ovule structure and developmental process in *A. thaliana*. **B**, DIC observation of ovules at Stage 3-VI. **C**, Confocal observation of ovules at Stage 3-VI. **D**, Quantification of normal and abnormal female gametophytes (FGs) at Stage 3-VI for each sample. The number of ovules observed is shown in [Supplemental Data](#) Set 1. Asterisks above the columns indicate significant differences compared to WT (** $P < 0.01$ by *t*-test). **E**, DIC (left panel) and confocal (right panel) observation of ovules at Stage 3-VI. **F**, Quantification of normal and abnormal FGs at Stage 3-VI for each sample. The number of ovules observed is shown in [Supplemental Data](#) Set 1. Different letters above the columns indicate significant differences at $P < 0.01$, as determined by one-way ANOVA. **G–I**, Signal corresponding to egg cell marker *pDD45:GFP* (**G**), central cell marker *pDD65:GFP* (**H**), and female gametophyte marker *pAKV:H2B-YFP* (**I**) in ovules at Stage 3-VI. **J–L**, The quantification of GFP/YFP signal intensity corresponding to egg cell marker *pDD45:GFP* (**J**), central cell marker *pDD65:GFP* (**K**), and female gametophyte marker *pAKV:H2B-YFP* (**L**) in WT and *arp6 er-119* mutant ovules at Stage 3-VI. Error bars indicate \pm SD ($n = 10$ biological replicates). Different letters above the columns indicate significant differences at $P < 0.01$, as determined by one-way ANOVA. cn, central cell nucleus; en, egg cell nucleus; sn, synergid cell nucleus. Bars in (**B**)–(**E**), 5 μ m. Bars in (**G**)–(**I**), 10 μ m. The female gametophyte is outlined by white dot lines in (**B**) and (**C**), (**E**), and (**G**)–(**I**).

Results

The SWR1 chromatin-remodeling complex genetically interacts with the ER-MPK-signaling pathway to control female gametophyte development

The SWR1 chromatin-remodeling complex was shown to regulate female meiosis during female gametophyte development (Rosa et al., 2013; Qin et al., 2014). Consistent with this regulatory function, in a subset of mature Stage 3-VI ovules (Schneitz et al., 1995), the SWR1 subunit single mutants showed abnormal female gametophytes at frequencies (57.6% in *pie1*, 51.2% in *arp6*, and 37.1% in *sef*) significantly higher than that in wild-type (WT; 0.5%, $P < 0.01$, see Supplemental Data Set 1 for statistical data). The mutants either lacked female gametophyte cell nuclei or contained smaller female gametophytes compared to wild-type ovules, which typically contained a kidney-shaped female gametophyte with a central cell, an egg cell, two synergid cells, and three antipodal cells nuclei (Figure 1A–D).

To identify additional genes involved in SWR1 control of female gametophyte development, we performed an EMS mutagenesis screen for enhancers of the *arp6* mutation. In this screen, we identified an *ERECTA* (*ER*) point mutation allele *er-119*, a C-to-T mutation resulting in the conversion of 397th amino acid in the LRR domain from Arg to a premature stop codon. *er-119* is a knock-out allele that significantly enhanced the fertility defects in *arp6* (Cai et al., 2017; Supplemental Figure S1A). The phenotype of *er-119* is similar to that of *er-105*.

To examine if the reduced fertility in *arp6 er-119* double mutants results from male or female tissues, we conducted reciprocal crosses and found that the low fertility of the *arp6 er-119* double mutant was specifically due to defects in the female tissues (Supplemental Figure S2A and B). An in vivo pollen tube guidance assay showed that many *arp6 er-119* ovules did not receive pollen tubes (Supplemental Figure S2C). Consistent with these findings, *arp6 er-119* showed a significantly increased percentage of developmentally stunted ovules with an abnormal female gametophyte, compared to the *arp6* and *er-119* single mutants (Figure 1E and F; $P < 0.01$, Supplemental Data Set 1).

To test if gamete cell differentiation is also affected in the *arp6 er-119* female gametophyte, we separately introduced egg cell, central cell, and female gametophyte cell markers into *arp6 er-119*. The *pDD45:GFP* egg cell marker, the *pDD65:GFP* central cell marker, and the *pAKV:H2B-YFP* female gametophyte marker were expressed in only 11.2%, 12.7%, and 11.6% of *arp6 er-119* ovules, respectively, significantly lower than that (98.5%, 98.6%, and 97.7%) in wild-type ovules (Figure 1G–I; $P < 0.01$, Supplemental Data Set 1). The GFP/YFP signal was significantly decreased in *arp6 er-119* compared to WT (Figure 1J–L; $P < 0.01$, Supplemental Data Set 1), suggesting that ARP6 and ER are required for the differentiation of the female gametophyte.

A complementation construct containing the genomic *ER* sequence restored the reduced seed set and female gametophyte defects of *arp6 er-119* to levels comparable to those

in *arp6* (Supplemental Figure S1A and B). This analysis confirmed that the enhanced female gametophyte defects of *arp6 er-119* were caused by the *er-119* mutation. A second *er* allele, *er-105*, similarly enhanced the gametophytic defects of *arp6*, further supporting the involvement of both ARP6 and ER in female gametophyte development. Specifically, the *arp6 er-105* double mutant had reduced seed set and an increased percentage of abnormal female gametophytes compared to *arp6* (Supplemental Figure S1A–D). To investigate whether ER functions specifically with the ARP6 subunit of the SWR1-remodeling complex in female gametophyte regulation, we generated the *sef er-105* double mutant. Compared to the *sef* single mutant, the double mutant had enhanced defects in seed set and female gametophyte development (Supplemental Figure S1A–D).

MPK3 and MPK6 act redundantly downstream of ER in multiple developmental processes, including ovule development (Pillitteri et al., 2007; Wang et al., 2008). To test if the MPK-signaling pathway also functions with the SWR1 complex in female gametophyte regulation, we generated the *arp6 mpk6* and *sef mpk6* double mutants. Similar to the *arp6 er*, *sef er*, and *er mpk6* double mutants, *arp6 mpk6* and *sef mpk6* double mutants had reduced fertility and enhanced female gametophyte defects compared to the *arp6* and *sef* single mutants (Supplemental Figure S1A–D), as indicated by abnormal expression of the female gametophyte marker and the central cell and egg cell markers (Supplemental Figure S3A–C). The GFP/YFP signal was significantly decreased in *arp6 mpk6* and *er-105 mpk6* compared to WT (Supplemental Figure S3D–F; $P < 0.01$, Supplemental Data Set 1). Collectively, these results link SWR1 and the ER-MPK-signaling pathway in the regulation of female gametophyte development.

SWR1 and ER-MPK coordinately repress *MIR398c* expression in ovules

Next, we focused on the identification of components downstream of both the SWR1 complex and the ER-MPK-signaling pathway in the regulation of female gametophyte development. As the SWR1 complex controls activation or repression of gene expression (Ojolo et al., 2018), we profiled changes in gene expression in *arp6 er-119* double mutant ovules. Specifically, we performed comparative RNA-seq analysis of wild type, *arp6*, *er-105*, and *arp6 er-119* ovules from Stage 2-III to Stage 3-VI (Cai et al., 2017). Because the female gametophyte defects in *arp6 er-119* ovules were significantly greater than in *arp6*, we focused only on genes with significantly altered expression (fold change ≥ 2 , FDR ≤ 0.05 ; Supplemental Data Set 2) in the *arp6 er-119* double mutant compared to *arp6*. Among the 55 differentially expressed genes, *MIR398c* was the only miRNA-encoding gene and ranked second in the list of genes with increased expression (Supplemental Data Set 2 and Figure 2A). Reverse transcription-quantitative PCR (RT-qPCR) confirmed the increased *MIR398c* transcript levels in *arp6 er-119* ovules compared to WT, *arp6*, and *er-105* ovules (Figure 2B).

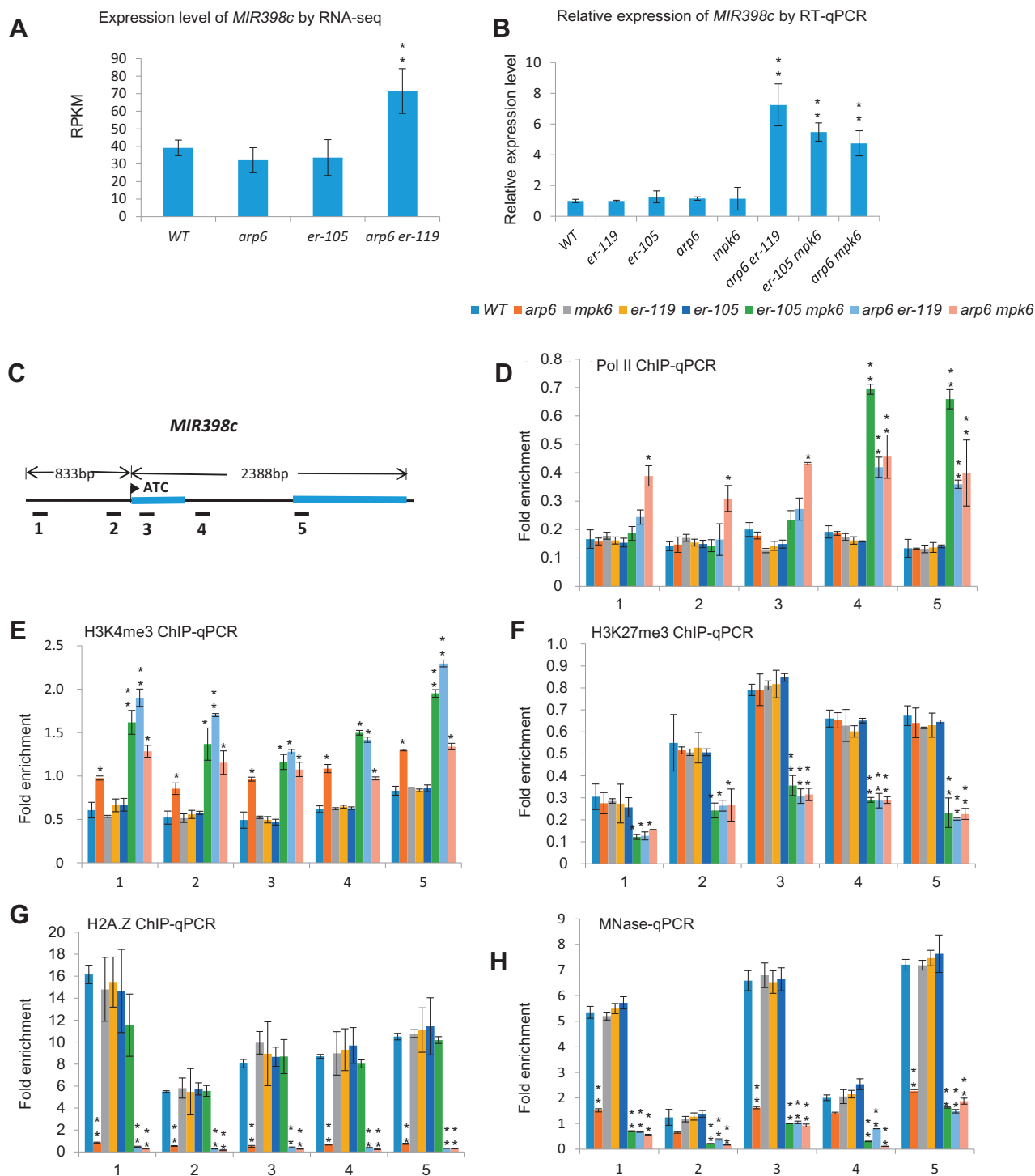


Figure 2 *MIR398c* transcription is repressed by SWR1 and the ER-MPK-signaling pathway. A, reads per kilobase per million mapped reads (RPKM) of *MIR398c* in ovules detected by RNA-seq. B, Relative *MIR398c* (pri-miR398c) levels in ovules tested by RT-qPCR analysis. C, Diagram of the *MIR398c* gene. Exons are indicated as blue boxes, and the promoter and introns are indicated as black lines. The flag indicates the transcription start site. Regions amplified by PCR primer sets are indicated with black bars below the diagram. Primer set numbers correspond to the numbers on the x-axis of the graphs in (D)–(H). D–G, Chromatin immunoprecipitation–quantitative polymerase chain reaction (ChIP-qPCR) analysis for the enrichment of RNA Pol II (D), H3K4me3 (E), H3K27me3 (F), and H2A.Z (G) at *MIR398c* in WT and the indicated mutants. H, Nucleosome occupancy at *MIR398c* as measured by MNase treatment followed by qPCR. Values are means \pm SD from three biological replicates. Each biological replicate corresponds to three technical replicates. Asterisks above the columns indicate significant differences compared to WT (** $P < 0.01$, * $P < 0.05$ by t test).

Similar increases in *MIR398c* expression were also detected in *arp6 mpk6* and *er-105 mpk6* double mutant ovules compared to WT, *arp6*, *er-105*, *er-119*, and *mpk6* ovules (Figure 2B), indicating that ARP6, ER, and MPK6 cooperatively repress *MIR398c* expression in ovules.

Because RNA polymerase II (Pol II) occupancy is a reliable indicator of active gene transcription, we compared Pol II occupancy at the *MIR398c* locus in WT, *arp6*, *er-119*, *er-105*, *mpk6*, *arp6 er-119*, *arp6 mpk6*, and *er-105 mpk6*. For this analysis, we performed chromatin immunoprecipitation followed by quantitative PCR (ChIP-qPCR) using floral bud tissues and a Pol II antibody. Pol II occupancy at the *MIR398c* gene body increased in *arp6 er-119*, *arp6 mpk6*, and *er-105 mpk6* compared to WT and each of the single mutants (Figure 2C and D). We also found that the abundance of H3K4me₃, a marker of active transcription, at *MIR398c* was significantly increased in *arp6 er-119*, *arp6 mpk6*, and *er-119 mpk6* (Figure 2C and E). Moreover, the H3K27me₃ repressive mark was significantly reduced at the *MIR398c* locus in the double mutants compared to wild type and the single mutants (Figure 2C and F). Together, these results demonstrate that *MIR398c* is actively transcribed in *arp6 er-119*, *arp6 mpk6*, and *er-105 mpk6*.

As a chromatin-remodeling complex, SWR1 regulates gene transcription by facilitating the deposition of the H2A.Z variant into nucleosomes and modifying histone-DNA interactions (Marques et al., 2010). To test if H2A.Z deposition at the *MIR398c* gene is mediated by ARP6, we performed ChIP-qPCR using an H2A.Z antibody. In wild-type floral buds, we detected a high level of H2A.Z deposition at the *MIR398c* promoter (Figure 2C and G). In contrast, H2A.Z occupancy at the *MIR398c* promoter was depleted in *arp6* floral buds, as well as *arp6 er-119* and *arp6 mpk6* floral buds (Figure 2C and G).

H2A.Z-containing nucleosomes have altered DNA interactions compared to H2A-containing nucleosomes, thereby affecting nucleosomal stability (Kumar and Wigge, 2010). We therefore evaluated nucleosome occupancy at *MIR398c* in the presence or absence of ARP6 using micrococcal nuclease (MNase) digestion followed by qPCR (Petesch and Lis, 2008). The results showed that nucleosome occupancy at regions occupied by H2A.Z was greatly decreased in the *arp6* single mutant and the *arp6 er-119* and *arp6 mpk6* double mutants, compared to wild type (Figure 2C and H). However, the activation of *MIR398c* transcription was only observed in the *arp6 er-119*, *arp6 mpk6*, and *er-105 mpk6* double mutants compared to wild type and not in the *arp6* single mutant (Figure 2A and B). The present findings therefore suggest that while SWR1 contributes to the transcriptional inhibition of *MIR398c*, a gene regulated by ER-MPK, changes in nucleosome status controlled by the SWR1 complex alone are not sufficient to alter *MIR398c* transcription.

MIR398c overexpression disrupted female gametophyte development

We next tested whether increased *MIR398c* expression leads to abnormal female gametophyte development. If *MIR398c* levels are increased in the double mutant ovules and if *MIR398c* expression is normally suppressed by SWR1 and ER, then *MIR398c* overexpression in wild type should recapitulate the female gametophyte defects of the *arp6 er* double mutants. To obtain *MIR398c* overexpression lines, we generated the constructs using the genomic *MIR398c* sequence driven by the constitutive *UBIQUITIN 10* (*UBQ10*) promoter (*pUBQ10:MIR398c-OE*) and the female gametophyte cell-specific AKV promoter (*pAKV:MIR398c-OE*) and transformed the constructs into wild-type plants, separately. RT-qPCR confirmed that *pUBQ10:MIR398c-OE* and *pAKV:MIR398c-OE* had increased *MIR398c* transcript levels (Figure 3A). Moreover, *pUBQ10:MIR398c-OE* and *pAKV:MIR398c-OE* plants had reduced fertility (Figure 3B) and abnormal female gametophytes (Figure 3C and D; significantly different from wild type, $P < 0.01$, Supplemental Data Set 1), which resembled the defects of the *arp6 er-119*, *er-105 mpk6*, and *arp6 mpk6* double mutants.

We also investigated whether knockout/knockdown of *MIR398c* could suppress the female gametophyte defects seen in *arp6 er-119* double mutants. A mutant line with a T-DNA insertion in the *MIR398c* locus (Dugas and Bartel, 2008) with reduced *MIR398c* transcripts (Supplemental Figure S4C), but without ovule development defects (Figure 3E and F), was crossed with the *arp6 er-119* double mutant to obtain *arp6 er-119 mir398c* plants. These plants had partially restored plant fertility and an increased percentage of normal female gametophytes compared to *arp6 er-119* (Figure 3E and F; $P < 0.01$, Supplemental Data Set 1). Together, these analyses show that elevated expression of *MIR398c* in *arp6 er* double mutants is sufficient to disrupt female gametophyte development.

miR398 target genes AGL51/52/78 act downstream of SWR1 and ER-MPK signaling in female gametophyte development

To investigate the molecular function of miR398 in female gametophyte development, we used the online tool psRNATarget (<http://plantgrn.noble.org/psRNATarget/>; Dai and Zhao, 2011) to identify putative miR398 targets. The identified candidate targets included three closely related AGAMOUS-LIKE (AGL) genes, *AGL51*, *AGL52*, and *AGL78*, which belong to the M β subclade of the MADS-box gene family (Parenicova et al., 2003). RT-qPCR analysis of *AGL51*, *AGL52*, and *AGL78* in wild type, *pUBQ10:MIR398c-OE*, *arp6*, and the ER-MPK pathway mutants showed that all three genes had reduced transcript levels in *pUBQ10:MIR398c-OE*, *arp6 er-119*, *arp6 mpk6*, and *er-105 mpk6* ovules compared to wild type and the single mutants (Figure 4A). We chose *AGL78* as a representative gene to confirm the bioinformatic miRNA target prediction using a modified 5'-RACE PCR technique that enables precise determination of the cleavage

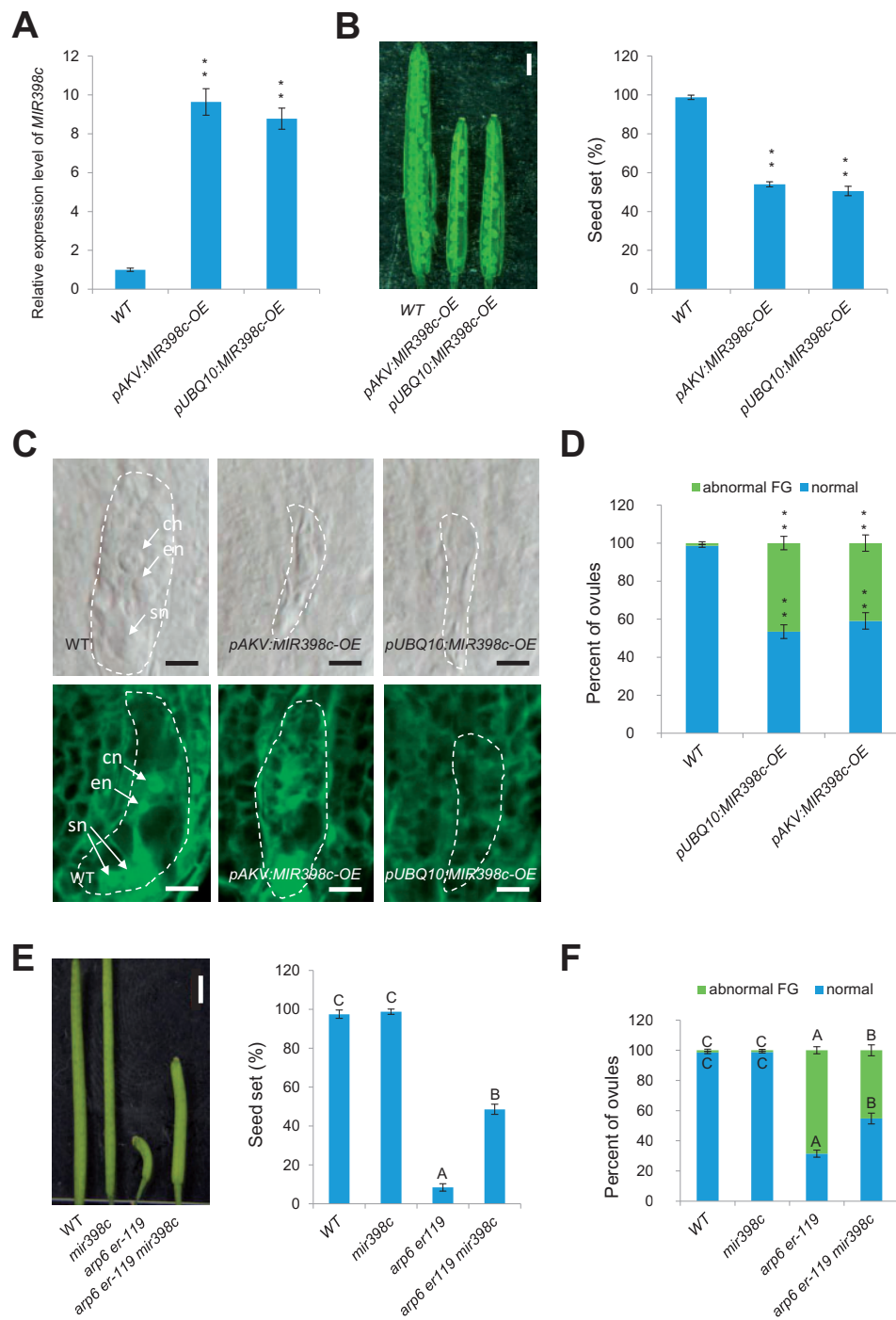


Figure 3 *MIR398c* acts downstream of *SWR1* and *ER* in female gametophyte regulation. **A**, Relative *MIR398c* levels in ovules of WT and *MIR398c* overexpression (OE) lines by RT-qPCR analysis. Data are means \pm SD ($n = 3$ biological replicates; $**P < 0.01$ by *t* test). **B**, Siliques (left panel) and quantification of seed-set percentage (right panel). Data are means \pm SD ($n = 10$ siliques from five independent plants, two independent siliques from each plant; $**P < 0.01$ by *t* test). Seed-set percentage was calculated corresponding to the percentage of aborted seeds/ovules. Bars = 1 mm. **C**, DIC (top panel) and confocal (bottom panel) observation of *MIR398c*-OE ovules at Stage 3-VI. cn, central cell nucleus; en, egg cell nucleus; sn, synergid cell nucleus. Bars = 5 μ m. The female gametophyte (embryo sac) is outlined by white dot lines. **D**, Quantification of female gametophyte phenotype at Stage 3-VI for each sample. The number of ovules observed is shown in Supplemental Data Set 1. $**$ Significant differences at $P < 0.01$ by *t* test. **E**, Siliques (left panel) and quantification of seed-set percentage (right panel). Data are means \pm SD ($n = 10$ biological replicates, 10 siliques from five independent plants, two independent siliques from each plant; different letters above the columns indicate statistically significant differences at $P < 0.01$, as determined by one-way ANOVA). Seed-set percentage was calculated corresponding to the percentage of aborted seeds/ovules. Bars = 1 mm. **F**, Quantification of female gametophyte phenotype at Stage 3-VI for each sample. The number of ovules observed is shown in Supplemental Data Set 1. Different letters above the columns indicate statistically significant differences at $P < 0.01$, as determined by one-way ANOVA.

sites of miRNAs on their mRNA targets (Llave et al., 2002). The results showed cleavage of *AGL78* mRNA within the predicted miR398 target site, between positions 10 and 11 of the miR398 nucleotides (Figure 4B).

We then tested whether loss of function of any of these three *AGL* genes would lead to compromised female gametophyte development. *agl78* had abnormal female gametophyte development and low seed set (Figure 4C–F), similar to the phenotypes of *MIR398c*-OE, *arp6 er-119*, *er-105 mpk6*, and *arp6 mpk6*. We also analyzed several gametophytic cell-specific GFP markers in *agl78*. The results showed that 23.9%, 20.3%, and 21.5% of *agl78* ovules did not properly express the *pAKV:H2B-YFP* (female gametophyte cells), *pDD45:GFP* (egg cell), and *pDD65:GFP* (central cell) markers, respectively (Figure 4G–I; significantly different from wild type, $P < 0.01$, Supplemental Data Set 1); also, the GFP/YFP signal was significantly decreased in *agl78* compared to WT (Figure 4J–L; $P < 0.01$, Supplemental Data Set 1). *agl78/+* heterozygous mutants, *agl51* and *agl52* single mutants, *agl51 agl52* double mutants, and *agl51/+ agl52/+* double heterozygous mutants did not exhibit female gametophyte defects (Figure 4C–F), but the *agl51* and *agl52* single mutations could enhance the female gametophyte and fertility defects of *agl78* in *agl51 agl78* and *agl52 agl78* double mutants (Figure 4C–F; $P < 0.01$, Supplemental Data Set 1). Taken together, these results suggest that increased miR398 accumulation in *ARP6* and *ER-MPK* pathway mutants disrupts normal female gametophyte development by inhibiting the expression of three redundant genes, *AGL51/52/78*, among which *AGL78* plays a dominant role in gametophyte development.

We conducted two experiments to test whether *AGL51/52/78* act downstream of *ARP6* and the *ER-MPK* pathway. First, we introduced a miR398-resistant form of *AGL78* driven by the native promoter and that contained five mutation sites (*pAGL78:AGL78m*; Figure 4B) into *arp6 er-119*. This line had significantly increased seed set and a reduced percentage of ovules with an abnormal female gametophyte compared to the *arp6 er-119* double mutant (Figure 4M and N; $P < 0.01$, Supplemental Data Set 1). Second, we overexpressed *AGL78* driven by the female gametophyte cell-specific *AKV* promoter in the *arp6 er-119* double mutant and found that it partially rescued the low seed set and female gametophyte defects of *arp6 er-119* (Figure 4O and P; $P < 0.01$, Supplemental Data Set 1). These data collectively indicate that *AGL51/52/78* function redundantly downstream of *ARP6* and the *ER-MPK* pathway to regulate female gametophyte development.

Expression pattern of *AGL51/52/78* and *MIR398c* in the developing ovule

Our results identified *AGL51/52/78* as positive regulators of female gametophyte development and *MIR398c* as a direct negative regulator of *AGL51/52/78* expression in ovules (Figure 4). However, the ovule is composed of both the diploid integument and haploid female gametophyte. We

therefore addressed the cell-specific spatial and temporal expression patterns of *AGL51/52/78* and *MIR398c* in ovules during female gametophyte development.

For *MIR398c*, we constructed a *MIR398c* promoter-GUS fusion (*pMIR398c:GUS*) and examined its expression in wild type. *pMIR398c:GUS* was expressed in the mature female gametophyte of ovules at Stage 3-VI, but not at earlier ovule stages such as 2-V and 3-I (Figure 5A). Consistent with the qPCR results (Figure 2B), *pMIR398c:GUS* expression in the female gametophyte of *arp6 er-119*, *arp6 mpk6*, and *er-105 mpk6* ovules showed two abnormalities. First, *pMIR398c:GUS* expression was significantly increased in the female gametophyte compared to the level in wild type, and *pMIR398c:GUS* was expressed at earlier stages of female gametophyte development such as 3-I (Figure 5A). The expression of *pMIR398c:GUS* in *arp6 +/- er-119 +/-* ovules is comparable to that in wild type (Supplemental Figure S5), suggesting that the regulation of *MIR398c* expression by *SWR1* and *ER*-signaling pathway likely act sporophytically. To investigate the expression pattern of *SWR1* and *ER* pathway genes in the ovule, we performed *pARP6:GUS* (Qin et al., 2014), *ER* in situ hybridization, and *pMPK6:MPK6-GFP* (Wang et al., 2008) expression analysis and found that *ARP6*, *ER*, and *MPK6* are expressed broadly in the ovule and present in both the female gametophyte and the ovule sporophytic tissue (Supplemental Figure S6).

To confirm the results of the *pMIR398c:GUS* reporter analysis, we performed ovule whole-mount in situ hybridization using an antisense *MIR398c* probe. The hybridization results confirmed the preferential expression of *MIR398c* in the mature wild-type female gametophyte and the increased expression of *MIR398c* in *arp6 er-119*, *arp6 mpk6*, and *er-105 mpk6* premature female gametophytes compared to wild type (Figure 5B). These results indicated that the combined activities of *SWR1* and *ER-MPK* are required to fully repress *MIR398c* expression in the early-stage megagametogenesis (Figure 5A and B). The mutations in *arp6 er-119*, *arp6 mpk6*, and *er-105 mpk6* also led to increased levels of *MIR398c* expression in the mature female gametophyte (Figure 5A and B), suggesting that *SWR1* and *ER-MPK* also regulate *MIR398c* expression levels at the mature female gametophyte stage.

The Arabidopsis genome contains three *MIR398* genes. In order to know whether *MIR398a* and *MIR398b* were also expressed in ovules, we constructed *pMIR398a:GUS* and *pMIR398b:GFP* transgenes and examined their expression patterns in ovules. *pMIR398a:GUS* was expressed in early-stage floral buds, but not in ovules (Supplemental Figure S7A). Whereas, *pMIR398b:GFP* was only expressed in the inner integument primordia or distal epidermal nucellus cells of ovules at meiosis stage (Stage 2-III; Supplemental Figure S7B). No signal was detected prior to Stage 2-II or post-meiosis (Supplemental Figure S7B). These data indicated that the expression patterns of *MIR398a* and *MIR398b* are different from that of *MIR398c*. We also found that either *mir398a* or *mir398b* mutation failed to restore fertility to

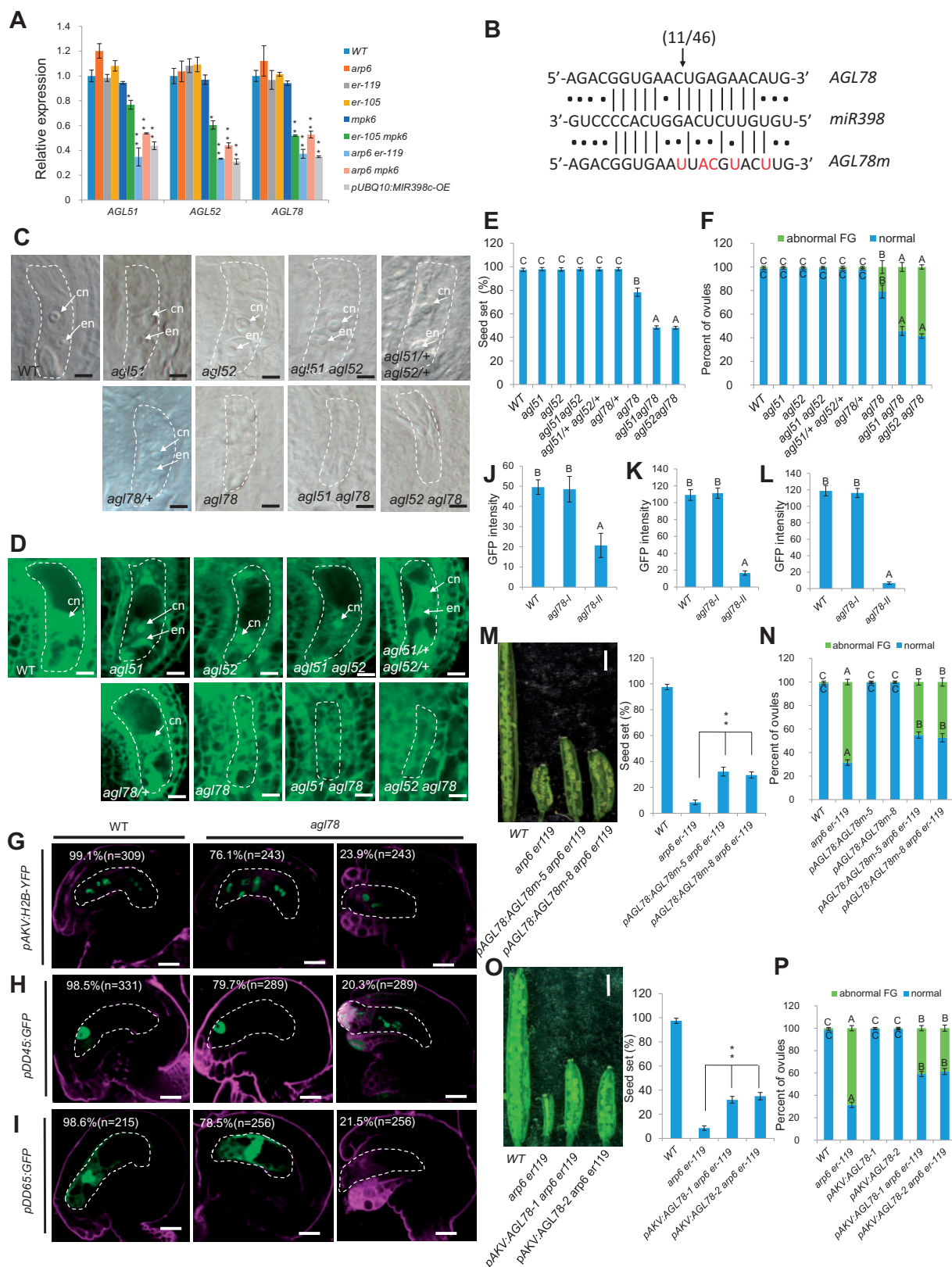


Figure 4 *AGL51/52/78*, targets of *miR398*, regulate female gametophyte development. **A**, Relative mRNA levels of *AGL51/52/78* in ovules by RT-qPCR analysis. Data represent means \pm SD ($n = 3$ biological replicates; ** $P < 0.01$, * $P < 0.05$ by t test). **B**, Alignment of the *miR398* sequence with the corresponding complementary site of *AGL78* and a *miR398*-resistant form of *AGL78* (*AGL78m*). The arrow indicates the 5' terminus cleavage product for the number of clones indicated. Cleavage was experimentally validated using 5'-RACE PCR. Red letters indicate the mutation sites of *AGL78m*. The lines represent base pairing; the dots represent nonpairing. **C**, DIC observation of WT and mutant ovules at Stage 3-VI. Bars

arp6 er-119, although the sequences of mature miR398a and miR398b are near identical or identical to miR398c (Supplemental Figure S4A–B, D–F).

To characterize the cell-specific expression of *AGL51/52/78* in ovules, we generated transgenic plants for each of the promoter-GUS fusion constructs, *pAGL51:GUS*, *pAGL52:GUS*, and *pAGL78:GUS*. The promoter activities of *AGL51/52/78* were detected in the developing female gametophyte from post-meiotic Stages 3-I to mature Stage 3-VI (Figure 5C). Consistent with these GUS reporter results and as expected from their predicted transcription factor activity (Parenicova et al., 2003), GFP translationally fused to each of the three AGL proteins (*pAGL51:AGL51-GFP*, *pAGL52:AGL52-GFP*, and *pAGL78:AGL78-GFP*) localized to the nuclei of female gametophyte cells at post-meiotic Stage 3-I to mature Stage 3-VI (Figure 5D). To further confirm the female gametophyte-specific expression of *AGL51/52/78* in ovules, we performed laser capture microdissection (LCM) of female gametophyte and surrounding sporophytic ovule tissue at the mature stage (Stage 3-VI) followed by real-time RT-PCR and found that the transcripts of *AGL51/52/78* in the mature stage ovule were mainly detected in the female gametophyte and barely detected in the sporophytic tissue (Supplemental Figure S8A). Consistently, whole-mount ovule in situ hybridization assay also showed *AGL78* signal only in the female gametophyte of wild-type ovule from post-meiotic Stage 3-I to mature Stage 3-VI, but not in the surrounding sporophytic ovule tissue (Supplemental Figure S8B).

To confirm that *AGL51/52/78* expression is controlled by *ARF6* and the ER-MPK pathway, we introduced *pAGL78:AGL78-GFP* (as a representative of the three AGLs analyzed) into *arp6 er-119*. The *pAGL78:AGL78-GFP* construct was sufficient to rescue the mutant phenotype in *agl78* (Supplemental Figure S9), suggesting that this

construct plays a role similar to that of endogenous *AGL78*. Compared to wild type, we detected a reduced expression of *pAGL78:AGL78-GFP* in *arp6 er-119* ovules from post-meiotic Stage 3-I to mature Stage 3-VI (Figure 5E). This finding is consistent with our results in *arp6 er-119* and *arp6 mpk6* ovules, in which both *pMIR398c:GUS* activity and *MIR398c* transcript levels were increased from Stage 3-I to mature Stage 3-VI (Figures 2B and 5A and B). Introduction of the miR398-resistant form of *AGL78* (*pAGL78:AGL78m-GFP*) into the *arp6 er-119* double mutant revealed that its expression was comparable in *arp6 er-119* and WT ovules (Figure 5E). Based on these results, we concluded that *ARF6* and the ER-MPK-signaling pathway activate *AGL51/52/78* expression in the developing female gametophyte by repressing *MIR398c* transcription.

SWR1 and the ER-MPK-signaling pathway are required to prevent miR398 accumulation in the developing female gametophyte

As described above, *pMIR398c:GUS* was expressed in the mature female gametophyte of ovules at Stage 3-VI (Figure 5A), which coincided with the expression of its targets *AGL51/52/78*, according to promoter activity and protein-GFP fusion analyses (Figure 5C and D). One possible explanation for this unexpected expression overlap is that precursor or mature miR398 may migrate away from the mature female gametophyte, where *MIR398c* is transcribed, and localize elsewhere. This putative migration would allow *AGL51/52/78* expression in the female gametophyte without inhibition by miR398.

To test this hypothesis, we examined the localization of mature miR398 in ovules by performing whole-mount ovule in situ hybridization assay with miR398 locked nucleic acid (LNA) oligonucleotide probes. In wild type, miR398 signal was not detected in ovules until Stage 3-VI (Figure 6A).

Figure 4 (Continued)

= 5 μ m. cn, central cell nucleus; en, egg cell nucleus; sn, synergid cell nucleus. D, Confocal observation of WT and mutant ovules at Stage 3-VI. Bars = 5 μ m. cn, central cell nucleus; en, egg cell nucleus. E, Quantification of seed-set percentage for each sample. Data are means \pm SD (n = 10 siliques from five independent plants, two independent siliques from each plant). Different letters above the columns indicate statistically significant differences at P < 0.01, as determined by one-way ANOVA. Seed-set percentage was calculated corresponding to the percentage of aborted seeds/ovules. F, Quantification of female gametophyte phenotype at Stage 3-VI for each sample. The number of ovules observed is shown in Supplemental Data Set 1. Different letters above the columns indicate statistically significant differences at P < 0.01, as determined by one-way ANOVA. G–I, Signal corresponding to the female gametophyte marker *pAKV:H2B-YFP* (G), egg cell marker *pDD45:GFP* (H), and central cell marker *pDD65:GFP* (I) in Stage 3-VI ovules. Bars = 10 μ m. J–L, The quantification of GFP/YFP signal intensity corresponding to egg cell marker *pDD45:GFP* (J), central cell marker *pDD65:GFP* (K), and female gametophyte marker *pAKV:H2B-YFP* (L) in WT and *agl78* mutant ovules at Stage 3-VI. Error bars indicate \pm SD (n = 10 biological replicates). Different letters above the columns indicate statistically significant differences at P < 0.01, as determined by one-way ANOVA. M, Siliques (left panel) and quantification of seed-set percentage (right panel). Data represent means \pm SD (n = 10 siliques from five independent plants, two independent siliques from each plant; $^{***}P$ < 0.01 by t test). Seed-set percentage was calculated corresponding to the percentage of aborted seeds/ovules. Bars = 1 mm. N, Quantification of female gametophyte phenotype at Stage 3-VI for each sample. The number of ovules observed is shown in Supplemental Data Set 1. Different letters above the columns indicate statistically significant differences at P < 0.01, as determined by one-way ANOVA. O, Siliques (left panel) and quantification of seed-set percentage (right panel). Data represent means \pm SD (n = 10 siliques from five independent plants, two independent siliques from each plant; $^{***}P$ < 0.01 by t test). Seed-set percentage was calculated corresponding to the percentage of aborted seeds/ovules. Bars = 1 mm. P, Quantification of female gametophyte phenotype at Stage 3-VI for each sample. The number of ovules observed is shown in Supplemental Data Set 1. Different letters above the columns

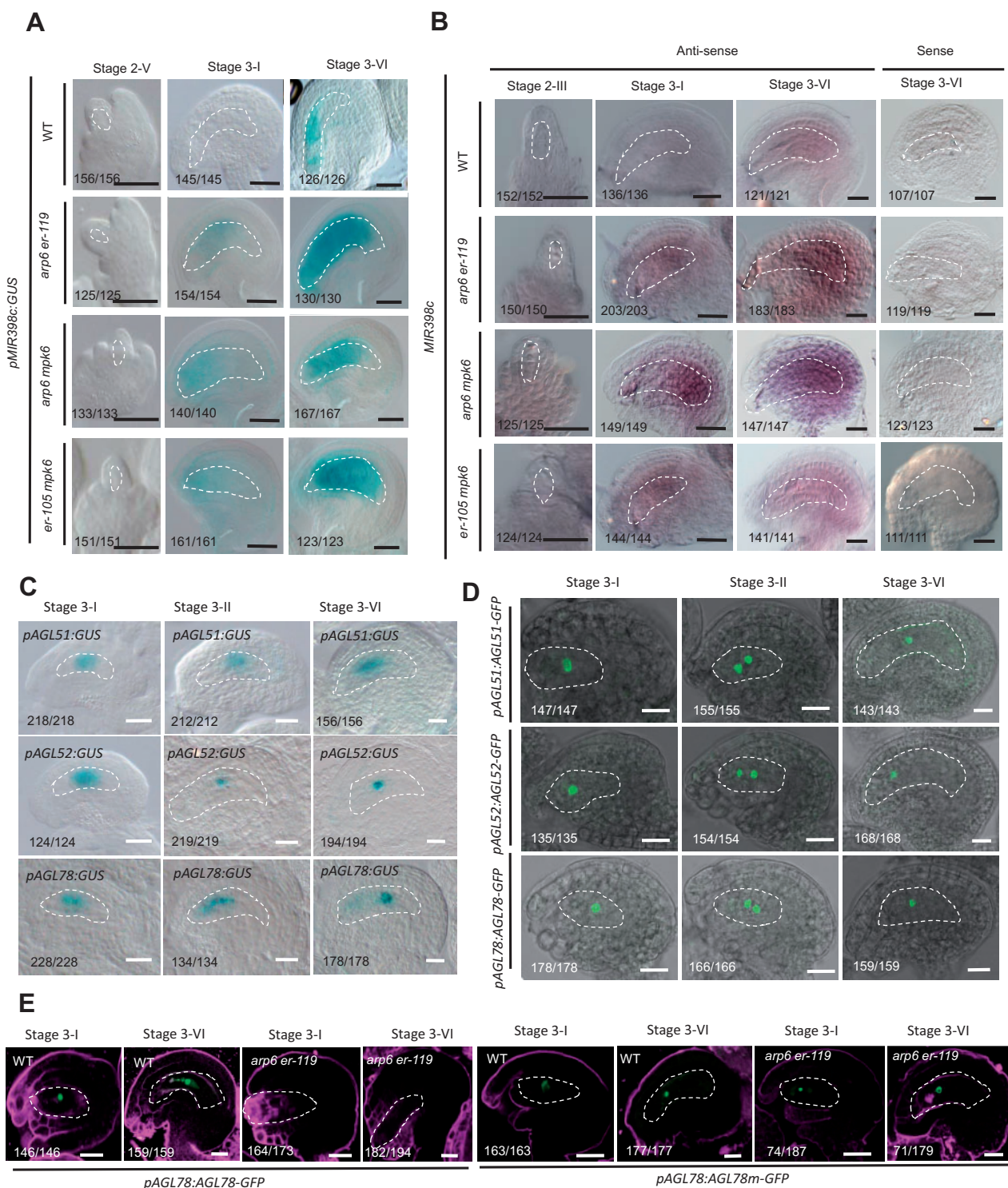


Figure 5 The expression pattern of *MIR398c* and *AGL51/52/78* in ovules. **A**, *pMIR398c:GUS* expression pattern in WT, *arp6 er-119*, *arp6 mpk6*, and *er-105 mpk6* ovules. Bars = 10 μ m. **B**, Whole-mount in situ hybridization of antisense and sense *MIR398c* probe in WT, *arp6 er-119*, *arp6 mpk6*, and *er-105 mpk6* ovules. Bars = 10 μ m. **C**, *pAGL51:GUS* (top row), *pAGL52:GUS* (middle row), and *pAGL78:GUS* (bottom row) expression pattern in ovules. Bars = 10 μ m. **D**, *pAGL51:AGL51-GFP* (top row), *pAGL52:AGL52-GFP* (middle row), and *pAGL78:AGL78-GFP* (bottom row) expression pattern in ovules. Bars = 10 μ m. **E**, Signal corresponding to *pAGL78:AGL78-GFP* and *pAGL78:AGL78m-GFP* expression in WT and *arp6 er-119* ovules. Bars = 10 μ m. The female gametophyte is outlined by white dot lines in (A)–(E).

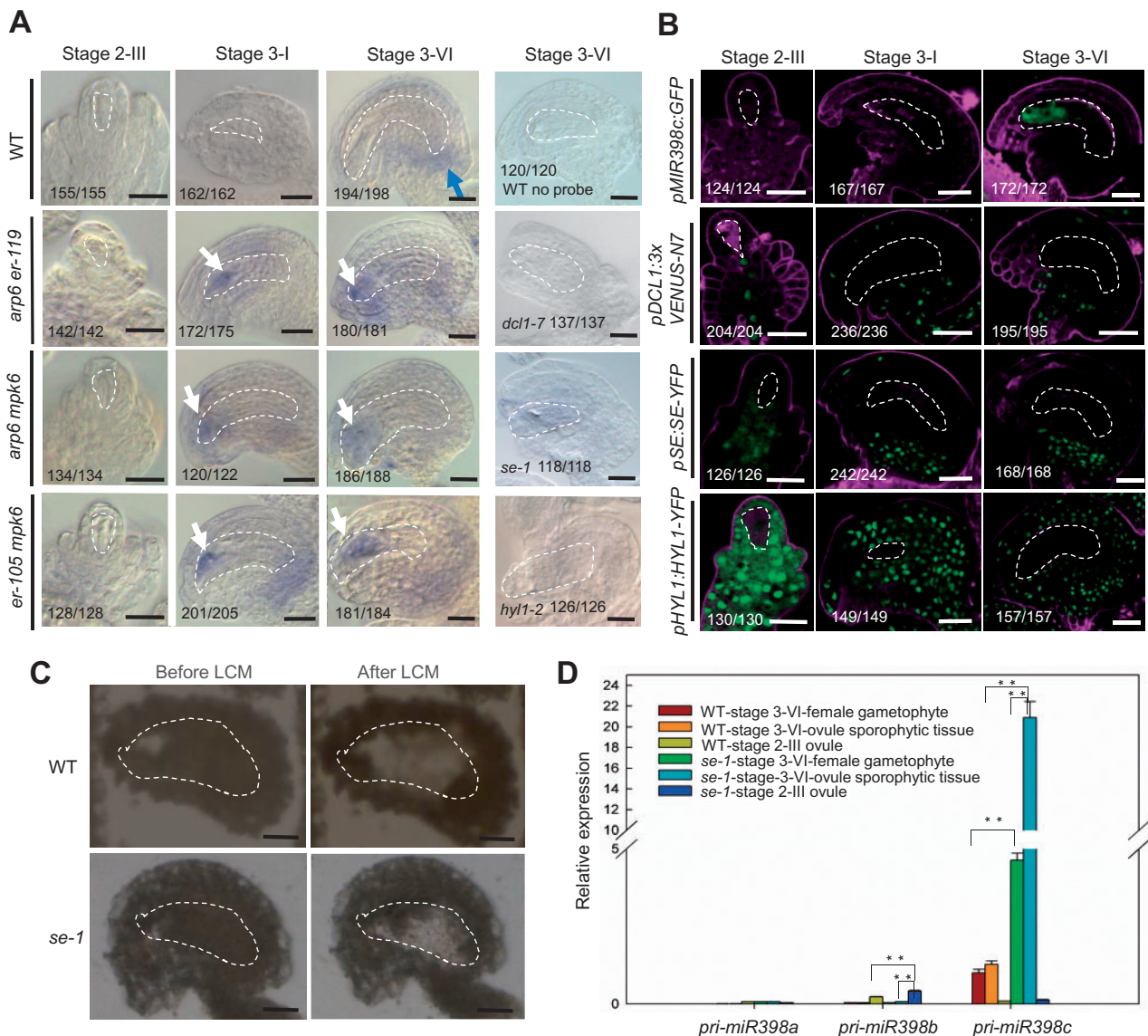


Figure 6 *pri-miR398c* is produced in the female gametophyte but is translocated to and processed in the surrounding sporophytic ovule tissues. A, Whole-mount ovule in situ localization of miR398 using LNA oligonucleotide probes. Blue arrow points to the chalaza-localized miR398 in WT. White arrows point to the ectopic localization of miR398 in the female gametophyte in the indicated mutants. B, Signal corresponding to *pMIR398c:GFP*, *pDCL1:3xVENUS-N7*, *pSE:SE-YFP*, and *pHYL1:HYL1-YFP* expression in ovules. C, Paraffin-embedded WT and *se-1* ovule at mature Stage 3-VI before and after LCM. D, Relative levels of *pri-miR398a/b/c* in LCM isolated female gametophyte and the surrounding sporophytic tissues of WT and *se-1* ovule at mature Stage 3-VI and the whole WT and *se-1* ovule at Stage 2–III undergoing meiosis tested by RT-qPCR analysis. Bars in (A)–(C), 10 μ m. Data are means \pm SD ($n = 3$ biological replicates; $**P < 0.01$ by *t* test). The female gametophyte is outlined by white dot lines in (A)–(C).

miR398 signal was detected in the chalaza of mature wild-type ovule, but not in the female gametophyte (Figure 6A), where *MIR398c* promoter activity was detected (Figure 5A). However, increased and ectopic miR398 signal was detected in the developing female gametophyte of *arp6 er-119*, *arp6 mpk6*, and *er-105 mpk6* double mutant ovules from the post-meiotic (Stage 3-I) to mature stages (Figure 6A). No miR398 signal was detected in wild-type ovules without probe, or in ovules of the miRNA-processing mutants *dcl1-7*, *se-1*, and *hyl1-2* with the miR398 LNA probe (Figure 6A).

The promoter-GUS activity and in situ hybridization analyses showed that the *MIR398c* gene was mainly transcribed in the female gametophyte, but that mature miR398 was present in the chalaza and not in the female gametophyte of wild-type ovules. Analysis using the *MIR398c* promoter-GFP fusion construct confirmed that *MIR398c* promoter activity was restricted to the female gametophyte at mature stage (Figure 6B), prompting us to investigate where miR398 is processed. To this end, we determined the expression patterns of genes that encode the microprocessor, which processes primary miRNAs (*pri-miRNAs*). These included

DICER-LIKE1 (DCL1, an RNase III enzyme), SERRATE (SE, a zinc finger protein), and HYPONASTIC LEAVES1 (HYL1, a dsRNA-binding protein). *DCL1*-promoter GFP fusion (*pDCL1:3* × *VENUS-N7*) is only expressed in the ovule-sporophytic tissue (Figure 6B). Similarly, for SE and HYL1, YFP fusions driven by native promoters (Fang and Spector, 2007) were detected exclusively in ovule sporophytic tissue and not in the female gametophyte (Figure 6B). SE-YFP was enriched in the chalaza (Figure 6B). Thus, the expression patterns of *MIR398c* and the microprocessor genes are mutually exclusive. To further determine whether the biogenesis of miR398 occurs in ovule sporophytic or gametophytic tissues, we performed in situ hybridization assay to detect mature miR398 in ovules from *dcl1-7* +/- plants. Although half of the female gametophyte is *dcl* mutant, 93.9% of ovules from a *dcl1-7* +/- plant ($n = 214$) exhibited miR398 signal in the chalaza (Supplemental Figure S10A), similar to that in WT (94.9%, $n = 178$), indicating that the processing of pri-miR398 does not occur in the female gametophyte. In line with this conclusion, phenotypes of *dcl1* mutants show maternal effects while homozygous *dcl1* mutants have reduced fertility, *dcl1* gametophytes do not show defects when the sporophyte is *dcl1*/+ (Golden et al., 2002; Supplemental Figure S10B–D).

We therefore hypothesize that pri-miR398c needs to be translocated from the female gametophyte to the surrounding sporophytic ovule tissues to be processed. To test this hypothesis, we performed LCM of the female gametophyte and surrounding sporophytic ovule tissue at the mature stage (Stage 3–VI) followed by real-time RT-PCR in wild type (Figure 6C). Although both *pMIR398c:GUS* and *pMIR398c:GFP* showed that pri-miR398c was mainly produced in the female gametophyte, we found that the level of pri-miR398c in the ovule sporophytic tissue at the mature stage was comparable to that in the female gametophyte (Figure 6D), suggesting that pri-miR398 was translocated from the female gametophyte to the surrounding ovule sporophytic tissues. No or very low levels of pri-miR398c were detected in the laser capture dissected whole ovule undergoing meiosis (Stage 2–III; Figure 6D), consistent with the results from *pMIR398c:GUS* and *pMIR398c:GFP* analysis. If pri-miR398c was produced in female gametophyte but translocated into the ovule sporophytic tissue for processing, then it is expected that in a miRNA-processing mutant, pri-miR398c would accumulate more in the ovule sporophytic tissue than in the female gametophyte. Indeed, we detected increased pri-miR398c in both *se-1* female gametophyte and *se-1* surrounding ovule sporophytic tissues at the ovule mature stage compared to wild type (Figure 6D). More importantly, the level of pri-miR398c in *se-1* ovule sporophytic tissue was significantly higher than that in *se-1* female gametophytes (Figure 6D). No or very low levels of pri-miR398a and pri-miR398b were detected in the laser capture dissected ovules (Figure 6D), consistent with previous *pMIR398a:GUS* and *pMIR398b:GFP* expression pattern analysis. Together these results suggest that pri-miR398c was

produced in the female gametophyte, but was translocated to and processed in the ovule sporophytic tissue. The movement of pri-miRNA and the sporophyte-specific expression pattern of the miRNA-processing proteins may serve as an efficient strategy to prevent the accumulation of miRNAs in the female gametophyte. The expression pattern of *HYL1-YFP* in wild type and *arp6 er-119* ovule is comparable (Supplemental Figure S11A and B), suggesting that SWR1 and the ER-MPK pathway may not affect pri-miRNA398c processing.

SWR1 and the ER-MPK-signaling pathway also activate AGO10 expression in the chalaza to sequester miR398

MiRNAs can move from cell to cell by passive diffusion (Carlsbecker et al., 2010) but an unknown gating mechanism can provide directionality in miRNA trafficking (Skopelitis et al., 2018). As mature miR398 accumulated in the chalaza, but not in the female gametophyte in WT ovule, we hypothesized that there may be a barrier that prevents mature miR398 from moving back to the female gametophyte. AGO10 has been shown to attenuate miR165/6 activity by sequestering the miRNA (Zhu et al., 2011), and to promote its degradation (Yu et al., 2017). Intriguingly, previous data showed that miR398 was the second most abundant miRNA species found in AGO10 immunoprecipitation (Yu et al., 2017). We thus examined the expression pattern of *pAGO10:YFP-AGO10* (Yu et al., 2017) in ovules and found that AGO10 was present in the chalaza of ovules from Stage 2–V to Stage 3–VI (Figure 7A), the tissue where miR398 is located.

This led to the hypothesis that AGO10 sequesters miR398 in the chalazal region. To test this hypothesis, we performed ovule whole-mount in situ hybridization with the miR398 LNA probe using the ovules of wild type and *pnh-2* (a loss-of-function *ago10* mutant; Liu et al., 2009). We observed expanded localization of miR398 in *pnh-2* ovules, in contrast to the chalaza-specific localization of miR398 in wild-type ovules (Figure 7B). These results demonstrate that AGO10 prevents the movement of miR398 to the female gametophyte by sequestering miR398 in the chalaza.

MiR398 was not detected in the wild-type female gametophyte but ectopically accumulated in the female gametophyte of *arp6 er-119*, *arp6 mpk6*, and *er-105 mpk6* double mutant ovules (Figure 6A). These findings prompted us to investigate how SWR1 and the ER-MPK pathway might repress the movement of mature miR398 to the female gametophyte. We therefore quantified the transcript levels of AGO10 in the ovules of wild type and the SWR1 and ER-MPK pathway mutants. RT-qPCR analysis showed that AGO10 transcripts were significantly decreased in the *arp6 er-119*, *arp6 mpk6*, and *er-105 mpk6* double mutants compared to wild type, *arp6*, *er-119*, *er-105*, and *mpk6* (Figure 7C). We also crossed *pAGO10:YFP-AGO10* into *arp6 er-119* and found that the expression of *pAGO10:YFP-AGO10*

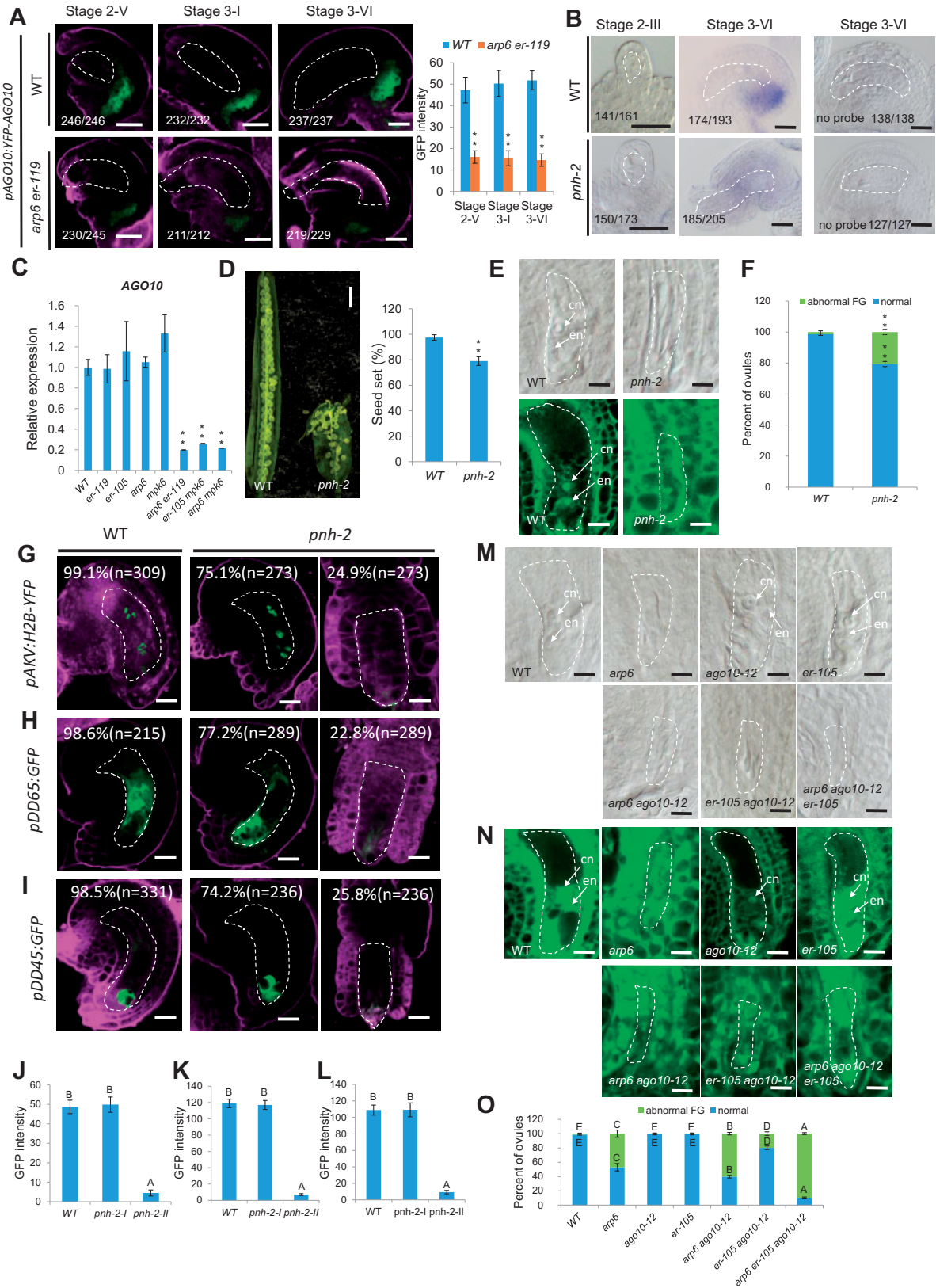


Figure 7 AGO10 expression activated by SWR1 and the ER-signaling pathway is required for the sequestration of miR398 in the chalaza. A, Signal corresponding to *pAGO10:YFP-AGO10* expression in WT and *arp6 er-119* ovules (left panel) and quantification of YFP signal intensity corresponding to *pAGO10:YFP-AGO10* in WT and *arp6 er-119* ovules (right panel). Error bars indicate \pm SD ($n = 10$ biological replicates; $**P < 0.01$ by t test). B, In situ localization of miR398 in WT and *pnh-2* ovules using miR398 LNA oligonucleotide probes. C, Relative mRNA levels of *AGO10* in ovules by RT-qPCR analysis. Data are means \pm SD ($n = 3$ biological replicates; $**P < 0.01$ by t test). D, Siliques (left panel) and quantification of seed-set

in *arp6 er-119* ovules was significantly reduced compared to wild type (Figure 7A), consistent with the RT-qPCR results.

The next question we addressed was whether AGO10 is required for ovule development. Analysis of the ovule morphology of *pnh-2* showed reduced fertility (Figure 7D), an aberrant female gametophyte (Figure 7E and F), as indicated by abnormal expression of the female gametophyte marker and the central cell and egg cell markers (Figure 7G–I; significantly different from wild type, $P < 0.01$, Supplemental Data Set 1) and the GFP/YFP signal was significantly decreased in *pnh-2* compared to WT (Figure 7J–L; $P < 0.01$, Supplemental Data Set 1), suggesting the involvement of AGO10 in female gametophyte development. We also introduced the weak point mutation allele *ago10-12* (Ji et al., 2011), which does not show any obvious female gametophyte developmental defects, into *arp6*, *er-105*, and *arp6 er-105* and observed severe ovule developmental defects in *arp6 ago10-12*, *er-105 ago10-12*, and *arp6 ago10-12 er-105* ovules (Figure 7M–O). These data indicate that SWR1 and the ER-MPK-signaling pathway also activate AGO10 expression to sequester miR398 in the chalaza to ensure proper female gametophyte development.

Female gametophyte-expressed AGL51/52/78 control sporophytic integument growth

In addition to the female gametophyte defects, we noted that integument growth was also compromised in the *agl78*, *agl51 agl78*, and *agl52 agl78* mutants. Considering that AGL51/52/78 were specifically expressed in the female gametophyte and not in sporophytic tissues in both developing and mature ovules (Figure 5C and D), these sporophyte integument defects were surprising. To test the possibility that female gametophyte-expressed AGL51/52/78 affect integument development, we characterized integument development in wild type and *agl* mutant ovules. In wild type, the female gametophyte was fully enveloped by integument tissue, which curled around the gametophyte to form a micropyle close to the funiculus (Supplemental Figure S12A and B). However, in a subset of *agl78*, *agl51 agl78*, and *agl52 agl78* mutant ovules, the integument did not elongate sufficiently to cover the female gametophyte; as a result, the micropyle did not bend as far as in wild type, leading to an

atypical protruding female gametophyte (Supplemental Figure S12A and B; $P < 0.01$, Supplemental Data Set 1). To determine whether the integument growth defect in the mutants was due to reduced cell proliferation, we stained mature Stage 3-VI ovules with Calcofluor White and quantified the integument cell numbers in the outermost layer. The results revealed significantly fewer cells in the outer integuments of *agl78*, *agl51 agl78*, and *agl52 agl78* compared to wild type (Supplemental Figure S12C and D; $P < 0.01$, Supplemental Data Set 1).

We performed two experiments to test whether miR398 and AGL51/52/78 are important for ovule sporophytic tissue development. First, we examined if *pUBQ10:MIR398c-OE* and *pAKV:MIR398c-OE* ovules exhibit integument growth defects. Indeed, we detected ovules with reduced integument growth and the protruding embryo sac phenotype (Supplemental Figure S12B), as well as reduced outer integument cell numbers in *pUBQ10:MIR398c-OE* and *pAKV:MIR398c-OE* ovules (Supplemental Figure S12B and D; significantly different to wild type, $P < 0.01$, Supplemental Data Set 1). Second, we knocked down *MIR398c* and induced AGL78 overexpression driven by native promoter or the female gametophyte cell-specific AKV promoter, and both approaches could complement the protruding female gametophyte and integument defects in *arp6 er-119* ovules, to varying degrees (Supplemental Figure S12C and D; Supplemental Data Set 1). These data indicate that in addition to regulating female gametophyte development, AGL51/52/78 also affects sporophytic integument growth.

Since *MIR398c* acts downstream of SWR1 and the ER-MPK pathway and since the movement of miR398 is dependent on SWR1 and ER-MPK, we investigated whether single and double *ARP6* and ER-MPK pathway mutants exhibit integument growth defects. The protruding female gametophyte phenotype was detected in the *pie1* and *pnh-2* single mutants, but the phenotype was very weak or not detected in the *arp6*, *sef*, *er-119*, and *er-105* single mutants (Supplemental Figures S12C and D, S13–S15). However, the *arp6 er-119*, *arp6 er-105*, *arp6 mpk6*, *er-105 mpk6*, *sef er-105*, *sef mpk6*, *arp6 ago10-12*, and *er-105 ago10-12* double mutants and *arp6 ago10-12 er-105* triple mutants all exhibited the protruding female gametophyte phenotype, and the

Figure 7 (Continued)

percentage (right panel) of WT and *pnh-2*. Data are means \pm SD ($n = 10$ siliques from five independent plants, two independent siliques from each plant; ** $P < 0.01$ by t test). Seed-set percentage was calculated corresponding to the percentage of aborted seeds/ovules. E, DIC (top panel) and confocal (bottom panel) observation of WT and *pnh-2* ovules at Stage 3-VI. F, Quantification of female gametophyte phenotype in WT and mutant at Stage 3-VI for each sample. The number of ovules observed is shown in Supplemental Data Set 1. (** $P < 0.01$ by t test). (G–I) Signal corresponding to the female gametophyte marker *pAKV:H2B-YFP* (G), the central cell marker *pDD65:GFP* (H), and the egg cell marker *pDD45:GFP* (I) in ovules at Stage 3-VI. J–L, The quantification of GFP/YFP signal intensity corresponding to female gametophyte marker *pAKV:H2B-YFP* (J) central cell marker *pDD65:GFP* (K) and egg cell marker *pDD45:GFP* (L) in WT and *pnh-2* mutant ovules at Stage 3-VI. Error bars indicate \pm SD ($n = 10$ biological replicates). Different letters above the columns indicate statistically significant differences at $P < 0.01$, as determined by one-way ANOVA. M, DIC observation of WT and mutant ovules at Stage 3-VI. N, Confocal observation of WT and mutant ovules at Stage 3-VI. O, Quantification of female gametophyte phenotype in WT and mutant at Stage 3-VI for each sample. The number of ovules observed was showed in Supplemental Data Set 1. Different letters above the columns indicate statistically significant differences at $P < 0.01$, as determined by one-way ANOVA. cn, central cell nucleus; en, egg cell nucleus. Bars in (A), and (B), 10 μ m; bar in (D), 1 mm; bars in (E), (M), and (N), 5 μ m; bars in (G)–(I), 10 μ m. The female gametophyte is outlined by white dot lines in (A), (B), (E), (G)–(I), (M), and (N).

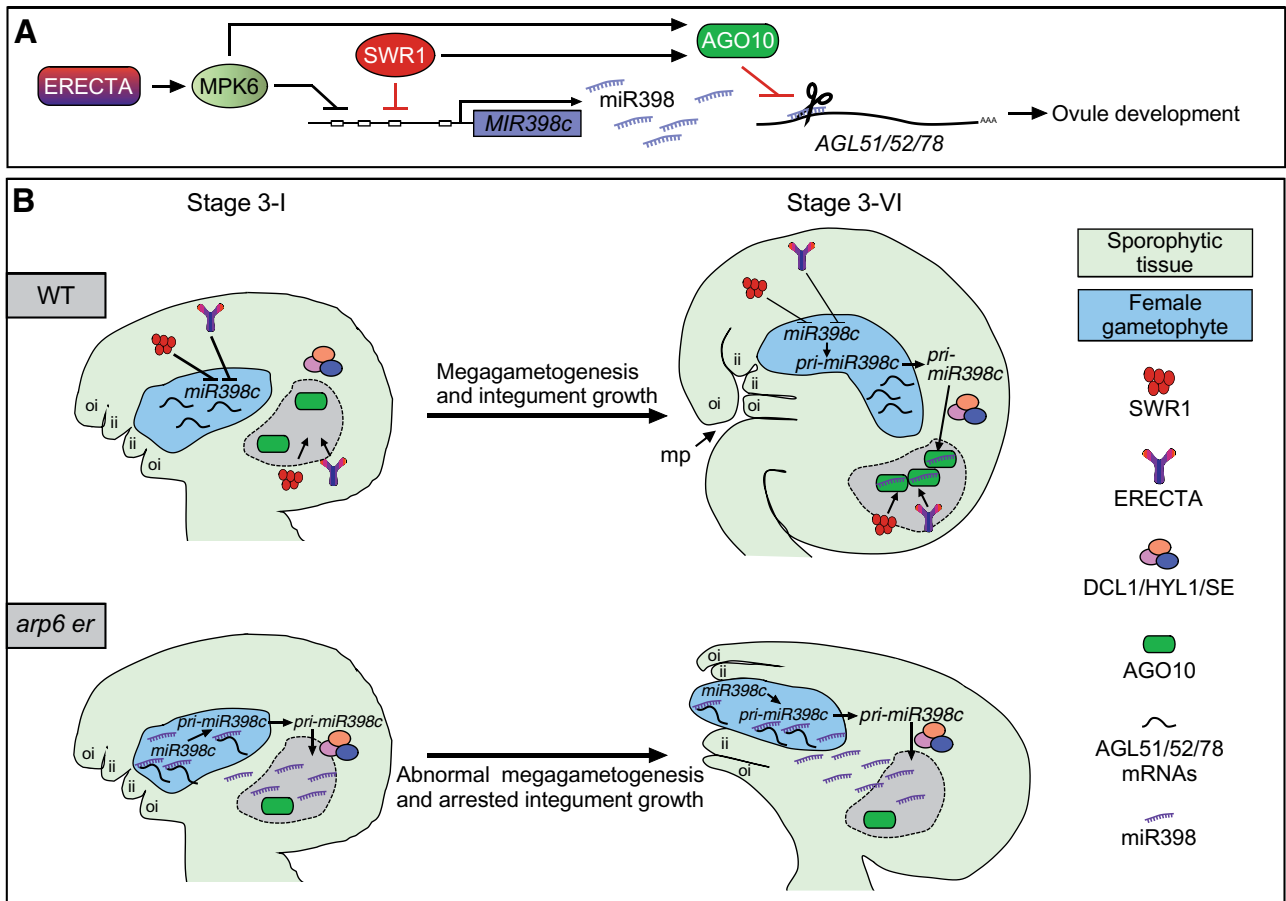


Figure 8 Proposed model for SWR1 coordination with ER signaling in regulating ovule development through the miR398-AGLs module. A, A diagram showing that SWR1 and ER–MPK6 repress the transcription of *MIR398c* and the accumulation of miR398. miR398 regulation of its target genes *AGL51/52/78* is attenuated by AGO10. The expression of AGO10 is promoted by SWR1 and ER–MPK6. B, A diagram showing the temporal and spatial control of miR398 biogenesis by SWR1 and ER to ensure female gametophyte development and proper ovule morphogenesis. In WT ovules, SWR1 and ER repress the transcription of *MIR398c* at the early stage of megagametogenesis. In the mature stage of ovule, pri-miR398c is transcribed in the female gametophyte. But, it is translocated from the female gametophyte to surrounding sporophytic tissues, where it is processed by DCL1, HYL1, and SE. SWR1 and ER–MPK6 also activate AGO10 expression in the chalaza, which is essential for sequestering miR398 and preventing its movement into the female gametophyte to access its targets *AGL51/52/78*. These AGLs are expressed in the female gametophyte and are essential for female gametophyte development as well as integument growth. In *arp6 er* ovules, increased *MIR398c* expression results in the over-accumulation of miR398. At the same time, the reduced AGO10 fails to sequester miR398, leading to ectopic accumulation of miR398 in the female gametophyte and inhibition of *AGL51/52/78* expression. As a result, these mutant ovules exhibit compromised female gametophyte development and a protruding embryo sac. The chalaza is labeled and outlined by black dot lines in B.

outer integument cell numbers were also significantly reduced in these double mutants compared to the single mutants and wild type (Supplemental Figure S12C and D and S13–S15; Supplemental Data Set 1). Taken together, these results indicate that SWR1 and the ER-MPK pathway control female gametophyte-specific *AGL51/52/78* expression, which in turn at least partially affects sporophytic integument growth in ovules.

Discussion

Coordinated cell expansion and cell proliferation are critical for plant growth and establishing organ shape. During ovule development, the coordinated growth of the sporophytic integuments and the gametophytic embryo sac required for ovule morphogenesis has long been believed to be regulated by active signaling events. Here, we provide developmental

genetic evidence that ER-MPK signaling, in coordination with the ATP-dependent chromatin-remodeling complex SWR1, regulates ovule development by inhibiting the transcription of pri-miR398 in early stage of megagametogenesis and preventing the accumulation of miR398 inside the female gametophyte (Figure 8). This work highlights the importance of coordination between signal transduction pathways and chromatin-remodeling factors in the temporal control of miRNA biogenesis and spatial control of miRNA distribution during development.

Coordinated activity of SWR1 and the ER-MAPK-signaling pathway controls ovule integument development by repressing *MIR398c* transcription

Although SWR1 has been shown to be involved in multiple growth and developmental processes (Aslam et al., 2019), it

remains unclear how SWR1 modulation of histone–DNA interactions controls gene transcription in specific developmental contexts. Here, we show that *MIR398c* expression was significantly increased in *arp6 er* and *arp6 mpk6* ovules but not in the *arp6* single mutant. Previous studies have shown that ARP6 plays a key role in female meiosis and ~45% of *arp6* ovules have meiotic defects, leading to abnormal female gametophyte development (Qin et al., 2014), which is associated with reduced recombinase *DISRUPTED MEIOTIC cDNA1 (DMC1)* expression, but not increased *MIR398c* expression. We revealed that the increased *MIR398c* expression and reduced *AGL51/52/78* expression cause the enhanced female gametophyte defects in *arp6 er* and *arp6 mpk6* double mutants. Therefore, the *pAGL78:AGL78m-GFP* and *pAGL78:AGL78m-GFP* constructs could only partially rescue the female gametophyte defects in the *arp6 er-119* double mutant. We also showed that overexpression of *AGL78* driven by the female gametophyte cell-specific *AKV* promoter also partially complements the *arp6 er-119* double mutant phenotype, indicating that miR398 target genes *AGL51/52/78* act downstream of ARP6 and the ER-MPK pathway in the control of ovule development.

We also found that the *arp6* mutation caused reduced H2A.Z and nucleosome occupancy at the *MIR398c* promoter. These observations indicate that through nucleosome dynamics, SWR1 contributes to the transcriptional inhibition of *MIR398c*, a gene regulated by ER-MPK. However, changes in nucleosome structure alone were not sufficient to alter *MIR398c* transcription. A recent study revealed that H2A.Z activates the expression of *MIR156a/MIR156c* in early shoot development (Xu et al., 2018), further indicating that SWR1 contributes to the fine control of plant development by maintaining a balance between miRNAs and their target mRNAs. In addition to altering nucleosome structure, H2A.Z also regulates gene transcription by affecting histone-modification status (Dai et al., 2017; Cai et al., 2019). Consistent with this role, we observed enhanced H3K4me3 and reduced H3K27me3 levels at *MIR398c*, alongside the reduced H2A.Z level in the *arp6* mutant. H2A.Z deposition at *MIR398c* was independent of ER-MPK signaling (Figure 2). A question for future study is how SWR1 and H2A.Z are specifically recruited at *MIR398c*.

The ER signal transduction pathway regulates ovule integument and female gametophyte development

MPK3/MPK6 and ER/ERL1/ERL2 regulate similar developmental processes in Arabidopsis. It was previously shown that the ovule integument defects of *mpk3 +/– mpk6 –/–* and *er1 erl2 +/–* mutants are due to disrupted cell proliferation, suggesting that the MPK3/MPK6 cascade might function downstream of ER family receptors in ovule patterning regulation (Pillitteri et al., 2007; Wang et al., 2008). In this study, we demonstrated that the MPK6 cascade functions in the same pathway as ER in the regulation of ovule morphology and promotes female gametophyte

development and integument cell proliferation. The YDA-MKK4/5-MPK3/6 cascade functions downstream of ER/ERLs in regulating inflorescence architecture by promoting cell division in pedicels, as demonstrated by epistasis analysis and gain- and loss-of-function analysis (Meng et al., 2012; Bemis et al., 2013). Correlative evidence also suggests the YDA-MKK4/5-MPK3/6 cascade is required to transduce the signals perceived by the ER receptor family in stomatal development and patterning (Wang et al., 2007; Kim et al., 2012; Pillitteri and Torii, 2012; Lampard et al., 2014). The YDA-MKK4/5-MPK3/6 module may similarly function downstream of ER in ovule development regulation.

Secreted EPF/EPFL peptides have been identified as ligands of ER receptors in multiple developmental processes (Abrash et al., 2011; Lee et al., 2012; Uchida et al., 2012). Given the large number of putative secreted proteins expressed in the developing ovule and the pivotal role of cell-cell communication in ovule development (Jones-Rhoades et al., 2007; Chevalier et al., 2011; Qu et al., 2015), it will be of interest to identify the ligands of the ER family in ovule development regulation. Components downstream of the ER-MPK cascade in stomatal development and substrates of MPK3/6 in stress responses and pollen development have been identified (Lampard et al., 2008; Bethke et al., 2009; Wang et al., 2010; Guan et al., 2014; Zhang et al., 2015). In contrast, the downstream components of the ER-MPK cascade in ovule integument development are largely unknown. Here, we show that the ER-MPK cascade is required to ensure the function of three redundant M β subclade MADS box genes *AGL51/52/78* in the female gametophyte. Specifically, it represses *MIR398c* transcription and inhibits miR398 accumulation in the female gametophyte via a gate-keeping mechanism (Figure 8).

MiR398 target genes *AGL51/52/78* regulate communication between the female gametophyte and surrounding sporophytic tissue to ensure proper ovule morphogenesis

The development of the haploid female gametophyte is tightly linked to the surrounding sporophyte (Yang and Sundaresan, 2000; Yadegari and Drews, 2004). Many sporophytic mutants with aberrant integument initiation and outgrowth, such as *bel1* (BELL1, a homeodomain TF; Reiser et al., 1995), *ino* (INNER NO OUTER, a YABBY TF; Villanueva et al., 1999), *ant* (an AP2 TF; Elliott et al., 1996; Klucher et al., 1996), *tsl* (TOUSLED, a nuclear Ser/Thr protein kinase; Roe et al., 1997), *hll* (HUELLENOS, a mitochondrial ribosomal protein; Schneitz et al., 1998), and *sin1/dcl1* (SHORT INTEGUMENTS1/DICER LIKE1, a ribonuclease; Robinson-Beers et al., 1992; Schauer et al., 2002) also exhibit arrested female gametophyte development, suggesting that integument formation promotes female gametophyte development. However, the effects of female gametophyte on the integument growth are less clear.

Here, we showed that *AGL51/52/78*, three M β subclade MADS-box genes (Parenicova et al., 2003) targeted by

miR398, are expressed in the developing female gametophyte. Loss-of-function mutations in *AGL51/52/78* disrupt female gametophyte development and inhibit integument cell proliferation, resulting in a protruding embryo sac and compromised ovule morphogenesis and fertility. The coordination of growth between the integuments and the female gametophyte is important for ovule morphogenesis and micropyle formation, which is essential for efficiently sending the attracting signal from the female gametophyte to pollen tube. The protruding female gametophyte phenotype in the double mutants including *arp6 er-119*, *arp6 er-105*, *arp6 mpk6*, *er-105 mpk6*, *sef er-105*, and *sef mpk6* could cause less successful targeting by pollen tubes. Therefore, greater reductions in seed set are found in double mutants, compared to the frequency of abnormal female gametophytes. Our findings underscore the importance of crosstalk between the female gametophyte and surrounding sporophytic integument tissues during ovule development.

Spatial specificity of pri-miRNA processing and sequestration of miRNAs in sporophytic tissue affect the regulation of target mRNAs

Small RNAs are key signals in plant development, growth, and stress responses (Liu and Chen, 2018). Recently, mobile small RNAs have been characterized as a positional signal to drive developmental patterning (Benkovics and Timmermans, 2014). For example, the specification of leaf adaxial-abaxial polarity, the specification of the root central stele, and the maintenance of shoot stem cell competency all rely on the movement of small RNAs (Juarez et al., 2004; Carlsbecker et al., 2010; Knauer et al., 2013). The movement of small RNAs, such as AGO9-associated 24-nucleotide small RNAs and *TAS3*-derived transacting small interfering RNAs (ta-siRNAs), has also been shown to be involved in the specification of the megaspore mother cell during the early stages of ovule development (Olmedo-Monfil et al., 2010; Su et al., 2017; Su et al., 2020). Despite the fundamental roles of mobile small RNAs in plant growth and survival, little is known about how their movement is precisely controlled. The proposed processes for the control of small RNA movement include the plasmodesmata, phloem-dependent mechanisms, and a gate-keeping mechanism (Han and Kim, 2016; Skopelitis et al., 2018; Tsikou et al., 2018).

By examining the expression pattern of the *MIR398c* and miRNA-processing proteins, we found that pri-miR398 is mainly generated in the female gametophyte, but is then translocated to and processed in the surrounding sporophytic tissue, likely in the proximal chalaza. In addition to the reported mature miRNA mobility during a developmental process and rhizobial infection (Skopelitis et al., 2018; Tsikou et al., 2018), here we showed that the pri-miRNA is also mobile. The female gametophyte-to-sporophytic translocation of pri-miRNA and the sporophyte-specific expression pattern of the miRNA-processing proteins may serve as an efficient strategy to prevent the accumulation of miRNAs in the female gametophyte. Although the *MIR398c*

promoter-GUS and -GFP fusions displayed female gametophyte-specific expression of pri-miR398c, some level of pri-miR398c signal in the ovule sporophytic tissues was detected by an in situ hybridization assay. The detection of pri-miR398c in the ovule sporophytic tissues could be due to the translocation of pri-miR398c from the female gametophyte to the ovule sporophytic tissues. The discrepancy could also be due to the absence of additional regulatory elements in the GUS and GFP fusions. Thus, the possibility of pri-miR398c production in the sporophyte is not completely ruled out. Nevertheless, based on the results from LCM followed by RT-qPCR analysis, gametophyte-to-sporophyte translocation of pri-miR398c is also not excluded.

AGO10 can lock or sequester miRNAs by preventing their normal regulatory roles, thereby helping to produce positional signals for multiple developmental processes (Manavella et al., 2011). The spatiotemporal sequestration of miR165/166 by AGO10 from their target HD-ZIP III genes in regulating shoot apical meristem maintenance was reported (Zhu et al., 2011; Zhou et al., 2015). In addition to association with miR165/166, AGO10 can also directly bind other miRNAs, including miR398 (Yu et al., 2017). Here, we further revealed that during ovule development, AGO10 sequesters miR398 in the chalaza to maintain the function of its target *AGL* genes in the female gametophyte. A recent study reported that miR165/166 also accumulates in the chalaza (Hashimoto et al., 2018), indicating that chalaza-localized AGO10 may serve as a gatekeeper that controls miRNA movement between the female gametophyte and sporophytic tissues. Notably, ectopic miR398 in the female gametophyte was detected in the *arp6 er-119*, *arp6 mpk6*, and *er-105 mpk6* double mutants. We demonstrate that AGO10 expression in the ovule chalaza is activated by SWR1 and the ER-MPK pathway, suggesting that AGO10 mediated sequestration of miR398 in chalaza is dependent on ARP6 and the ER-MPK-signaling pathway, providing new insights into the mechanisms underlying small RNA movement during plant development and the reciprocal communication between these tissues.

Materials and methods

Plant material and growth conditions

The *Arabidopsis thaliana* ecotype Columbia (Col) was used as wild type. All mutants are in the Col background except for *ago10-12* (*hen6*), which is in the Landsberg (*Ler*) background. The mutants and alleles used in this study were *arp6* (Qin et al., 2014), *sef* (CS822749), *pie1* (*Salk_096434*), *agl51* (*Salk_011841C*), *agl52* (*Salk_030570C*), *agl78* (*Salk_020476C*), *mir398a* (CS433641), *mir398b* (*SALK_122007*), *mir398c* (*Salk_038698C*), *dcl1-7* (CS3089), *se-1* (CS3257), *hyl1-2* (*SALK_064863*); from the Arabidopsis Biological Resource Center; ABRC), *er-105* (Shpak et al., 2005), *mpk6* (Liu and Zhang, 2004; Wang et al., 2007), *pnh-2* (Liu et al., 2009), and *ago10-12* (Ji et al., 2011). Plants were grown under 16 h light/8 h dark at 22°C.

Differential interference contrast observation of ovule structure

Ovules from WT, mutant, and transgenic plants were dissected from the pistils of Stages 8–13 flowers in a drop of chloral hydrate solution (chloral hydrate:H₂O:glycerol = 8:2:1; Zhao et al., 2014). Cleared ovules were observed under a differential interference contrast (DIC) microscope and imaged using a ZEISS (Imager.A2) microscope with DIC optics.

Preparation of ovules for confocal laser scanning microscopy

For confocal fluorescence microscopy, ovules were prepared according to a previously reported method (Christensen et al., 1997) and mounted in 30% glycerol with 5 μ M FM4-64 dye. The ovules were stained for 5 min and analyzed using a Leica TCS SP8 microscope.

Integument cell number counts

Ovules were analyzed after staining with a 0.1% solution of Calcofluor White for cell wall examination (Adamski et al., 2009) and imaged using a Leica SP8 confocal microscope. Cell number in the outmost layer of the outer integument was counted from the distal end (micropylar ends) to the proximal end (chalazal end). Significant differences were calculated by one-way ANOVA ($P < 0.01$; $n = 6$).

Plasmid construction

The *pMIR398c:GFP/GUS* constructs were generated by amplifying a 2-kb sequence upstream of the *MIR398c* gene from WT genomic DNA using the primers listed in Supplemental Table S1. The PCR product was cloned into the pENTR/D-TOPO vector (Invitrogen). pENTR/D-TOPO clones were recombined into the destination vectors pGWB604 (Nakagawa et al., 2007) and pGWB533 (Nakagawa et al., 2007) using LR Clonase II (Invitrogen). The PCR fragments were cloned into the pENTR/D-TOPO vector (Invitrogen), and the pENTR/D-TOPO clones were recombined into the destination vector pGWB502 (Nakagawa et al., 2007) using LR Clonase II (Invitrogen). *pMIR398a:GUS* and *pMIR398b:GFP* were generated by amplifying 681-bp and 608-bp upstream of the *MIR398a* and *MIR398b* gene sequences, respectively, from WT genomic DNA using the primers listed in Supplemental Table S1.

The PCR fragments were cloned into the pENTR/D-TOPO vector (Invitrogen), and the pENTR/D-TOPO clones were recombined into the destination vector pGWB533 and pGWB604 using LR Clonase II (Invitrogen). *pAGL51:GUS*, *pAGL52:GUS*, and *pAGL78:GUS* were generated by amplifying 1452-bp, 1594-bp, and 1490-bp upstream of the *AGL51/52/78* genes, respectively, from WT genomic DNA using the primers listed in Supplemental Table S1. The PCR products were cloned into the pENTR/D-TOPO vector (Invitrogen). pENTR/D-TOPO clones were recombined into the destination vector pGWB533 using LR Clonase II (Invitrogen). *pAGL51:AGL51-GFP*, *pAGL52:AGL52-GFP*, *pAGL78:AGL78-GFP*, and *pAGL78:AGL78m:GFP* were generated by amplifying 2040 bp, 2581-bp, 2513-bp, and 2513-bp sequences,

respectively, from WT genomic DNA and cDNA using the primers listed in Supplemental Table S1. The PCR products were cloned into the pENTR/D-TOPO vector (Invitrogen). pENTR/D-TOPO clones were recombined into the destination vector pGWB604 using LR Clonase II (Invitrogen). *pAGL78:AGL78* was generated by amplifying a 2516-bp sequence from WT genomic DNA using the primers listed in Supplemental Table S1. The PCR product was cloned into the pENTR/D-TOPO vector (Invitrogen). pENTR/D-TOPO clones were recombined into the destination vector pGWB502 using LR Clonase II (Invitrogen). The PCR product was cloned into the pENTR/D-TOPO vector (Invitrogen). pENTR/D-TOPO clones were recombined into the destination vector pGWB518 (Nakagawa et al., 2007) using LR Clonase II (Invitrogen). *pUBQ10:MIR398c* was generated by amplifying a 638-bp sequence of UBQ10 promoter from WT genomic DNA and a 2375 bp of the *MIR398c* gene sequences using the primers listed in Supplemental Table S1. The PCR product was cloned into the pENTR/D-TOPO vector (Invitrogen). pENTR/D-TOPO clones were recombined into the destination vector pGWB501 (Nakagawa et al., 2007) using LR Clonase II (Invitrogen). *pAKV:AGL78* was generated by amplifying a 1854-bp sequence of AKV promoter from WT genomic DNA and a 1026-bp sequence of *AGL78* CDS from cDNA using the primers listed in Supplemental Table S1. The PCR product was cloned into the pENTR/D-TOPO vector (Invitrogen). pENTR/D-TOPO clones were recombined into the destination vector pGWB501 using LR Clonase II (Invitrogen). The *pER:ER* construct was generated by amplifying a 7634-bp segment of *ER* genomic DNA using the primers listed in Supplemental Table S1. The PCR product was then cloned into pENTR/D-TOPO vector (Invitrogen) and recombined into the destination vectors pGWB404 using LR Clonase II (Invitrogen). *pAKV:MIR398c* was generated by amplifying an 1854-bp sequence of AKV promoter from WT genomic DNA and a 2375 bp of the *MIR398c* gene sequences using the primers listed in Supplemental Table S1. The PCR product was cloned into the pENTR/D-TOPO vector (Invitrogen). pENTR/D-TOPO clones were recombined into the destination vector pGWB501 using LR Clonase II (Invitrogen). *pDCL1:3 × VENUS-N7* were generated by amplifying 2000-bp upstream of the *DCL1* gene sequence from WT genomic DNA using the primers listed in Supplemental Table S1. The PCR fragments were cloned into the pSPL4 3xVENUS-N7 vector with BamHI and XbaI restriction sites (Heisler et al., 2005).

Generation of transgenic plants and marker lines in WT or mutants background

The GV3101-Agrobacterium with the *pER:ER* or *AGL78*-relative complementation vectors was used to transform the *arp6 +/– er-119 +/–* double heterozygote, and the transformants were selected by respective antibiotics. The *arp6 er-119* double homozygote plants with the *pER:ER* or *AGL78*-relative complementation vectors were genotyped and

selected. At least 10 independent lines were obtained for every complementation construct. The GV3101-*Agrobacterium* with the *pUBQ10:MIR398c* or *pAKV:MIR398c* vectors was used to transform the WT, and the transformants were identified by selecting seedlings on Murashige and Skoog (MS) plates containing hygromycin at $50 \mu\text{gml}^{-1}$. At least 10 independent T3 homozygous lines were used for phenotypic characterization. The overexpression lines were selected and established with similar methods, and T3 generation plants were used for phenotypic analysis. Various female gametophyte-specific marker lines were introgressed into the *arp6 er-119*, *arp6 mpk6*, *er-105 mpk6*, *agl78*, and *pnh-2* background by crossing homozygous mutant plants to the marker lines and allowing the F1 to self-fertilize. PCR genotyping of the segregating F2 population was performed, and the marker gene was identified under a fluorescence microscope. F3 homozygous plants (mutant and marker lines both homozygous) were used in this study. The homozygous status of the plants was confirmed by the corresponding antibiotic selection marker in the transgene and Mendelian inheritance segregation ratios of the selection markers. At least 10 independent F3 generation lines crossed with markers were obtained for phenotypic analysis.

RNA-seq and analysis of differentially expressed genes

Ovaries with ovules from Stage 2-III to Stage 3-VI were collected from Stage 8 to Stage 12 WT, *arp6*, *er-105*, and *arp6 er-119* flower buds. RNA isolation, sequencing, and data processing were conducted as previously described (Zhao et al., 2014). We used the TAIR10 Arabidopsis thaliana genome as the reference. Clean reads were aligned to the reference genome using STAR v2.5.0. The alignment results were processed using the SourceForge Subread package featureCount v1.5.0 for gene quantification. Finally, edgeR v3.12.0 was used to identify the differentially expressed genes (fold change ≥ 2 ; a value of FDR ≤ 0.05 was considered to be statistically significant) between samples.

RT-qPCR

The RNA samples were extracted from WT and mutants' ovaries (with ovules from Stage 2-III to Stage 3-VI). In order to determine the relative transcript levels of selected genes, real-time qPCR was performed with specific primers (Supplemental Table S1) according to manufacturer' instructions using the BIO-RAD real-time PCR system and the SYBR Premix Ex Taq II system (TaKaRa), and the details were described (Cai et al., 2017). The expression levels were analyzed by the Livak method (Livak and Schmittgen, 2001). Data are represented as the normalized relative expression level ($2^{-\Delta\Delta\text{CT}}$) of the respective genes in various samples. The relative transcript levels of the analyzed genes were normalized to the transcript levels of *HK2* (AT4G26410; Cai et al., 2017). Three biological replicates and two technical replicates for each sample were performed in the qPCR experiments.

In situ hybridization of whole-mount ovules

Ovules with placenta were dissected from Stage 8 to 12 pistils, fixed, and processed as previously described (Hejatko et al., 2006; Javelle and Timmermans, 2012). For the *MIR398c* and *AGL78* probe, 299-bp and 263-bp fragments were cloned into the pTA2 vector (Toyobo), respectively. The PCR primers used are listed in Supplemental Table S1. PCR products were amplified using ExTaq DNA polymerase, and then cloned into the linearized pTA2 vector. For in situ localization of small RNAs, LNA oligonucleotide probes were used. *miR398* DIG-labeled LNA probe was ordered directly from Exiqon (<http://www.exiqon.com/microrna-in-situ-Hybridization>).

ChIP-qPCR

ChIP was performed as previously described (Qin et al., 2014) using inflorescences with floral buds younger than 12c stage. Polyclonal H2A.Z antibodies (Deal et al., 2007), Pol II antibodies (Abcam, ab817), anti-H3K27me3 (Millipore, 07-449), and anti-H3K4me3 (Millipore, 07-473) were used. The relative enrichment of H2A.Z, H3K27me3, H3K4me3, and Pol II-associated DNA fragments was analyzed by qPCR as previously described (Qin et al., 2014). Our previous genome-wide analysis of the distribution patterns of H2A.Z, H3K4me3, H3K27me3 mark, and nucleosome occupancy had shown that H2A.Z regulates gene expression by modulating nucleosome structure at +1 nucleosome and -1 nucleosome in association with H3K4me3 and H3K27me3 (Dai et al., 2017). Therefore, the five regions (1 to 5) of the *MIR398c* locus across the promoter, -1 nucleosome, +1 nucleosome, and gene body were selected for ChIP-qPCR analysis. ChIP experiments results were calculated by the Fold Enrichment Method. Fold Enrichment value was obtained as follows: ChIP fraction Ct value for the normalized background (NIS/mock IP) fraction Ct value (first $\Delta\Delta\text{Ct}$), $\Delta\Delta\text{Ct} [\text{CHIP/NIS}] = \Delta\text{Ct} [\text{normalized CHIP}] - \Delta\text{Ct} [\text{normalized NIS/mock}]$. Fold Enrichment = $2(-\Delta\Delta\text{Ct} [\text{CHIP/NIS}])$; Cai et al., 2019). Fold enrichment of ChIP experiments was calculated using *HK2* (AT4G26410) gene as a reference. Primers used in ChIP-qPCR are listed in Supplemental Table S1.

Nucleosome occupancy

MNase digestion of enriched chromatin followed by qPCR was performed as previously described (Kumar and Wigge, 2010) with minor modifications. Oligos were designed to have 95–110-bp amplicons every 35–45 bp in *MIR398c*. Chromatin from inflorescences with floral buds younger than 12c stage was digested with MNase, and mononucleosome-sized fragments were gel purified and used in qPCR. Relative nucleosome occupancy was represented as the fraction of uncut chromatin DNA and was plotted against the *MIR398c* gene positions relative to the transcription start sites (TSS) for each primer pair; the position denotes the center of each amplicon. Oligonucleotide sequences used are provided in Supplemental Table S1.

5'-RACE PCR

To experimentally validate computationally predicted miRNA targets, 5'-RACE PCR was performed (Nadiya et al., 2018). The ligated product was reverse transcribed using 5'-RACE outer primer complementary to the linker and a gene-specific outer primer, followed by PCR amplification using 5'RACE inner primer and gene-specific inner primer. RACE products were purified using the Agarose Gel DNA Purification Kit (TaKaRa Bio), ligated into the pMD18-T vector (TaKaRa Bio), and sequenced. Gene-specific primers used are listed in Supplemental Table S1.

LCM

Ovaries from WT and *se-1* mutant with ovules at mature Stage 3-VI and meiosis Stage 2-III fixed, embedded, and processed as previously described (Tang et al., 2012). TargetAmp™ 2-Round aminoallyl-aRNA amplification kit 1.0 (Epicentre, TAA2R4924) and Qiagen RNeasy MinElute Cleanup Kit (Qiagen, 74204), SuperScript II Reverse Transcriptase (Invitrogen, 18064-014), and SuperScript III Reverse Transcriptase (Invitrogen, 18064-044) were used for RNA amplification.

GUS staining

Inflorescence samples or pistils pollinated with *pLAT52:GUS* pollen and *pMIR398c:GUS* transgenic plant inflorescence and ovules samples were fixed, stained, and processed as previously described (Cai et al., 2017). After the staining, the ovules were observed under a ZEISS (Imager.A2) microscope.

Statistical analysis

All *t*-test analysis was conducted using Excel and the ANOVA analysis was conducted using SPSS software. To determine statistical significance, we employed independent *t*-tests with two-tail distribution between two groups and one-way ANOVA Turkey's test among various genotypes. A value of $P < 0.05$ was considered to be statistically significant. The results of statistical analyses are shown in Supplemental Data Set 1.

Accession numbers

Sequence data from this article can be found in the Arabidopsis Genome Initiative or GenBank/EMBL databases under the following accession numbers: *ARP6* (AT3G33520), *ERECTA* (AT2G26330), *PIE1* (AT3G12810), *SEF* (AT5G37055), *MPK6* (AT2G43790), *MIR398a* (AT2G03445), *MIR398b* (AT5G14545), *MIR398c* (AT5G14565), *AGL78* (AT5G65330), *AGL51* (AT4G02235), *AGL52* (AT4G11250), *AGO10* (AT5G43810), *DCL1* (AT1G01040), *HYL1* (AT1G09700), and *SE* (AT2G27100). The RNA-seq data are deposited in the European Nucleotide Archive under accession number PRJEB42278.

Supplemental data

Supplemental Figure S1. SWR1 and ER-MPK pathway double mutants exhibited low seed set and compromised female gametophyte development.

Supplemental Figure S2. The reduced seed set of *arp6 er-119* is due to female defects.

Supplemental Figure S3. The expression of the female gametophyte marker (*pAKV:H2B-YFP*), central cell marker *pDD65:GFP*, and egg cell marker *pDD45:GFP* is altered in *arp6 mpk6* and *er-105 mpk6* ovules.

Supplemental Figure S4. The functions of *MIR398a* and *MIR398b* are different from *MIR398c*.

Supplemental Figure S5. The expression of *pMIR398c:GUS* in *arp6 +/- er-119 +/-* ovule at Stage 3-VI is comparable to that in wild type.

Supplemental Figure S6. The expression of *ARP6*, *ER*, and *MPK6* in the ovules.

Supplemental Figure S7. The expression patterns of *MIR398a* and *MIR398b* in flower buds and ovules.

Supplemental Figure S8. The expression pattern of *AGL51/52/78* in female gametophyte.

Supplemental Figure S9. The *pAGL78:AGL78-GFP* construct is sufficient to complement the fertility defects in *agl78*.

Supplemental Figure S10. *dcl1-7 +/-* heterozygote exhibited normal phenotype in ovule structure and plant fertility.

Supplemental Figure S11. The expression of *pHYL1:HYL1-YFP* is not affected in *arp6 er-119*.

Supplemental Figure S12. *AGL51/52/78* and *MIR398c* also regulate sporophytic integument growth.

Supplemental Figure S13. The *er-119* mutation enhanced the integument growth defects in SWR1 complex mutants.

Supplemental Figure S14. *AGO10* regulates sporophytic integument growth.

Supplemental Figure S15. The *ago10* mutation enhanced the integument growth defects of the *arp6 er* mutant.

Supplemental Table S1. Primers used in this study.

Supplemental Data Set 1. The comparison and statistical results.

Supplemental Data Set 2. RNA-seq expression values of the differentially expressed genes (DEGs) in *arp6 er-119* double mutant ovules compared to *arp6*.

Acknowledgments

We thank Dr. K. Torii for sharing the *er-105* seeds and Dr. R. Deal for sharing the H2A.Z antibody. We thank Dr. W. Tang for providing the LCM platform and technical guidance.

Funding

This work was supported by NSFC (grant nos. 31970333, U1605212 to Y.Q.; 31700279 to H.C.), Guangxi Distinguished Experts Fellowship and Science and Technology Major Project of Guangxi (Gui Ke 2018-266-Z01) to Y.Q., and NIH GM129373 to X.C.

Conflict of interest statement: The authors declare no competing interests.

References

- Abrash EB, Davies KA, Bergmann DC** (2011) Generation of signaling specificity in Arabidopsis by spatially restricted buffering of ligand-receptor interactions. *Plant cell* **23**: 2864–2879.
- Adamski NM, Anastasiou E, Eriksson S, O'Neill CM, Lenhard M** (2009) Local maternal control of seed size by KLUH/CYP78A5-dependent growth signaling. *Proc Natl Acad Sci USA* **106**: 20115–20120.
- Armenta-Medina A, Huanca-Mamani W, Sanchez-Leon N, Rodriguez-Arevalo I, Vielle-Calzada JP** (2013) Functional analysis of sporophytic transcripts repressed by the female gametophyte in the ovule of Arabidopsis thaliana. *PLoS One* **8**: e76977.
- Aslam M, Fakher B, Jakada BH, Cao S, Qin Y** (2019) SWR1 chromatin remodeling complex: a key transcriptional regulator in plants. *Cells* **8**:1621
- Baker SC, Robinson-Beers K, Villanueva JM, Gaiser JC, Gasser CS** (1997) Interactions among genes regulating ovule development in Arabidopsis thaliana. *Genetics* **145**: 1109–1124.
- Bemis SM, Lee JS, Shpak ED, Torii KU** (2013) Regulation of floral patterning and organ identity by Arabidopsis ERECTA-family receptor kinase genes. *J Exp Bot* **64**:5323–5333.
- Bencivenga S, Colombo L, Masiero S** (2011) Cross talk between the sporophyte and the megagametophyte during ovule development. *Sex Plant Reprod* **24**:113–121.
- Bencivenga S, Simonini S, Benkova E, Colombo L** (2012) The transcription factors BEL1 and SPL are required for cytokinin and auxin signaling during ovule development in Arabidopsis. *Plant Cell* **24**: 2886–2897.
- Benkovics AH, Timmermans MC** (2014) Developmental patterning by gradients of mobile small RNAs. *Curr Opin Genet Dev* **27**: 83–91.
- Berr A, McCallum EJ, Menard R, Meyer D, Fuchs J, Dong A, Shen WH** (2010) Arabidopsis SET DOMAIN GROUP2 is required for H3K4 trimethylation and is crucial for both sporophyte and gametophyte development. *Plant Cell* **22**: 3232–3248.
- Bethke G, Unthan T, Uhrig JF, Poschl Y, Gust AA, Scheel D, Lee J** (2009) Flg22 regulates the release of an ethylene response factor substrate from MAP kinase 6 in Arabidopsis thaliana via ethylene signaling. *Proc Natl Acad Sci USA* **106**: 8067–8072.
- Cai H, Zhang M, Chai M, He Q, Huang X, Zhao L, Qin Y** (2019) Epigenetic regulation of anthocyanin biosynthesis by an antagonistic interaction between H2A.Z and H3K4me3. *New Phytol* **221**: 295–308.
- Cai H, Zhao L, Wang L, Zhang M, Su Z, Cheng Y, Zhao H, Qin Y** (2017) ERECTA signaling controls Arabidopsis inflorescence architecture through chromatin-mediated activation of PRE1 expression. *New Phytol* **214**:1579–1596.
- Carlsbecker A, Lee JY, Roberts CJ, Dettmer J, Lehesranta S, Zhou J, Lindgren O, Moreno-Risueno MA, Vaten A, Thitamadee S, et al.** (2010) Cell signalling by microRNA165/6 directs gene dose-dependent root cell fate. *Nature* **465**: 316–321.
- Carter B, Henderson JT, Svedin E, Fiers M, McCarthy K, Smith A, Guo C, Bishop B, Zhang H, Riksen T, et al.** (2016) Cross-talk between sporophyte and gametophyte generations is promoted by CHD3 chromatin remodelers in Arabidopsis thaliana. *Genetics* **203**: 817–829.
- Cheng CY, Mathews DE, Schaller GE, Kieber JJ** (2013) Cytokinin-dependent specification of the functional megaspore in the Arabidopsis female gametophyte. *Plant J* **73**: 929–940.
- Chevalier E, Loubert-Hudon A, Zimmerman EL, Matton DP** (2011) Cell-cell communication and signalling pathways within the ovule: from its inception to fertilization. *New Phytol* **192**:13–28.
- Choi K, Park C, Lee J, Oh M, Noh B, Lee I** (2007) Arabidopsis homologs of components of the SWR1 complex regulate flowering and plant development. *Development* **134**: 1931–1941.
- Choi K, Kim S, Kim SY, Kim M, Hyun Y, Lee H, Choe S, Kim SG, Michaels S, Lee I** (2005) SUPPRESSOR OF FRIGIDA3 encodes a nuclear ACTIN-RELATED PROTEIN6 required for floral repression in Arabidopsis. *Plant Cell* **17**: 2647–2660.
- Choi K, Zhao X, Kelly KA, Venn O, Higgins JD, Yelina NE, Hardcastle TJ, Ziolkowski PA, Copenhaver GP, Franklin FC, et al.** (2013) Arabidopsis meiotic crossover hot spots overlap with H2A.Z nucleosomes at gene promoters. *Nat Genet* **45**: 1327–1336.
- Christensen CA, King EJ, Jordan JR, Drews GNJSR** (1997) Megagametogenesis in Arabidopsis wild type and the Gf mutant. *Sexual Plant Reproduct* **10**: 49–64
- Coen O, Fiume E, Xu W, De Vos D, Lu J, Pechoux C, Lepiniec L, Magnani E** (2017) Developmental patterning of the sub-epidermal integument cell layer in Arabidopsis seeds. *Development* **144**: 1490–1497.
- Colombo M, Masiero S, Vanzulli S, Lardelli P, Kater MM, Colombo L** (2008) AGL23, a type I MADS-box gene that controls female gametophyte and embryo development in Arabidopsis. *Plant J* **54**: 1037–1048.
- Dai X, Zhao PX** (2011) psRNATarget: a plant small RNA target analysis server. *Nucleic Acids Res* **39**:W155–W159.
- Dai X, Bai Y, Zhao L, Dou X, Liu Y, Wang L, Li Y, Li W, Hui Y, Huang X, et al.** (2017) H2A.Z represses gene expression by modulating promoter nucleosome structure and enhancer histone modifications in Arabidopsis. *Mol Plant* **10**:1274–1292.
- Deal RB, Kandasamy MK, McKinney EC, Meagher RB** (2005) The nuclear actin-related protein ARP6 is a pleiotropic developmental regulator required for the maintenance of FLOWERING LOCUS C expression and repression of flowering in Arabidopsis. *Plant Cell* **17**: 2633–2646.
- Deal RB, Topp CN, McKinney EC, Meagher RB** (2007) Repression of flowering in Arabidopsis requires activation of FLOWERING LOCUS C expression by the histone variant H2A.Z. *Plant Cell* **19**: 74–83.
- Dugas DV, Bartel B** (2008) Sucrose induction of Arabidopsis miR398 represses two Cu/Zn superoxide dismutases. *Plant Mol Biol* **67**: 403–417.
- Elliott RC, Betzner AS, Huttner E, Oakes MP, Tucker WQ, Gerentes D, Perez P, Smyth DR** (1996) AINTEGUMENTA, an APETALA2-like gene of Arabidopsis with pleiotropic roles in ovule development and floral organ growth. *Plant Cell* **8**:155–168.
- Fang Y, Spector DL** (2007) Identification of nuclear dicing bodies containing proteins for microRNA biogenesis in living Arabidopsis plants. *Curr Biol* **17**: 818–823.
- Golden TA, Schauer SE, Lang JD, Pien S, Mushegian AR, Grossniklaus U, Meinke DW, Ray A** (2002) SHORT INTEGUMENTS1/SUSPENSOR1/CARPEL FACTORY, a Dicer homolog, is a maternal effect gene required for embryo development in Arabidopsis. *Plant Physiol* **130**: 808–822.
- Guan Y, Meng X, Khanna R, LaMontagne E, Liu Y, Zhang S** (2014) Phosphorylation of a WRKY transcription factor by MAPKs is required for pollen development and function in Arabidopsis. *PLoS Genet* **10**: e1004384.
- Han X, Kim JY** (2016) Integrating hormone- and micromolecule-mediated signaling with plasmodesmal communication. *Mol Plant* **9**: 46–56.
- Hashimoto K, Miyashima S, Sato-Nara K, Yamada T, Nakajima K** (2018) Functionally diversified members of the mir165/6 gene family regulate ovule morphogenesis in Arabidopsis thaliana. *Plant Cell Physiol* **59**: 1017–1026.
- Heisler MG, Ohno C, Das P, Sieber P, Reddy GV, Long JA, Meyerowitz EM** (2005) Patterns of auxin transport and gene expression during primordium development revealed by live imaging of the Arabidopsis inflorescence meristem. *Curr Biol* **15**: 1899–1911.

- Hejatko J, Blilou I, Brewer PB, Friml J, Scheres B, Benkova E** (2006) In situ hybridization technique for mRNA detection in whole mount Arabidopsis samples. *Nat Protoc* **1**: 1939–1946.
- Javelle M, Timmermans MC** (2012) In situ localization of small RNAs in plants by using LNA probes. *Nat Protoc* **7**: 533–541.
- Ji L, Liu X, Yan J, Wang W, Yumul RE, Kim YJ, Dinh TT, Liu J, Cui X, Zheng B, et al.** (2011) ARGONAUTE10 and ARGONAUTE1 regulate the termination of floral stem cells through two microRNAs in Arabidopsis. *PLoS Genet* **7**: e1001358.
- Johnston AJ, Meier P, Gheyselinck J, Wuest SE, Federer M, Schlagenhauf E, Becker JD, Grossniklaus U** (2007) Genetic subtraction profiling identifies genes essential for Arabidopsis reproduction and reveals interaction between the female gametophyte and the maternal sporophyte. *Genome Biol* **8**: R204.
- Jones-Rhoades MW, Borevitz JO, Preuss D** (2007) Genome-wide expression profiling of the Arabidopsis female gametophyte identifies families of small, secreted proteins. *PLoS Genet* **3**: 1848–1861.
- Juarez MT, Kui JS, Thomas J, Heller BA, Timmermans MC** (2004) microRNA-mediated repression of rolled leaf1 specifies maize leaf polarity. *Nature* **428**: 84–88.
- Kim TW, Michniewicz M, Bergmann DC, Wang ZY** (2012) Brassinosteroid regulates stomatal development by GSK3-mediated inhibition of a MAPK pathway. *Nature* **482**: 419–422.
- Kinoshita-Tsujimura K, Kakimoto T** (2011) Cytokinin receptors in sporophytes are essential for male and female functions in Arabidopsis thaliana. *Plant Signal Behav* **6**: 66–71.
- Klucher KM, Chow H, Reiser L, Fischer RL** (1996) The AINTEGUMENTA gene of Arabidopsis required for ovule and female gametophyte development is related to the floral homeotic gene APETALA2. *Plant Cell* **8**:137–153.
- Knauer S, Holt AL, Rubio-Somoza I, Tucker EJ, Hinze A, Pisch M, Javelle M, Timmermans MC, Tucker MR, Laux T** (2013) A proto-dermal miR394 signal defines a region of stem cell competence in the Arabidopsis shoot meristem. *Dev Cell* **24**:125–132.
- Kumar SV, Wigge PA** (2010) H2A.Z-containing nucleosomes mediate the thermosensory response in Arabidopsis. *Cell* **140**: 136–147.
- Lampard GR, Macalister CA, Bergmann DC** (2008) Arabidopsis stomatal initiation is controlled by MAPK-mediated regulation of the bHLH SPEECHLESS. *Science* **322**: 1113–1116.
- Lampard GR, Wengier DL, Bergmann DC** (2014) Manipulation of mitogen-activated protein kinase signaling in the Arabidopsis stomatal lineage reveals motifs that contribute to protein localization and signaling specificity. *Plant Cell* **26**: 3358–3371.
- Lazaro A, Gomez-Zambrano A, Lopez-Gonzalez L, Pineiro M, Jarillo JA** (2008) Mutations in the Arabidopsis SWC6 gene, encoding a component of the SWR1 chromatin remodeling complex, accelerate flowering time and alter leaf and flower development. *J Exp Bot* **59**: 653–666.
- Lee JS, Kuroha T, Hnilova M, Khatayevich D, Kanaoka MM, McAbee JM, Sarikaya M, Tamerler C, Torii KU** (2012) Direct interaction of ligand-receptor pairs specifying stomatal patterning. *Genes Dev* **26**: 126–136.
- Lituiev DS, Krohn NG, Muller B, Jackson D, Hellriegel B, Dresselhaus T, Grossniklaus U** (2013) Theoretical and experimental evidence indicates that there is no detectable auxin gradient in the angiosperm female gametophyte. *Development* **140**: 4544–4553.
- Liu L, Chen X** (2018) Intercellular and systemic trafficking of RNAs in plants. *Nat Plants* **4**: 869–878.
- Liu Q, Yao X, Pi L, Wang H, Cui X, Huang H** (2009) The ARGONAUTE10 gene modulates shoot apical meristem maintenance and establishment of leaf polarity by repressing miR165/166 in Arabidopsis. *Plant J* **58**: 27–40.
- Liu Y, Zhang S** (2004) Phosphorylation of 1-aminocyclopropane-1-carboxylic acid synthase by MPK6, a stress-responsive mitogen-activated protein kinase, induces ethylene biosynthesis in Arabidopsis. *Plant Cell* **16**: 3386–3399.
- Livak KJ, Schmittgen TD** (2001) Analysis of relative gene expression data using real-time quantitative PCR and the 2⁻(Delta Delta C(T)). *Methods* **25**: 402–408.
- Llave C, Xie Z, Kasschau KD, Carrington JC** (2002) Cleavage of Scarecrow-like mRNA targets directed by a class of Arabidopsis miRNA. *Science* **297**: 2053–2056.
- Luo YX, Hou XM, Zhang CJ, Tan LM, Shao CR, Lin RN, Su YN, Cai XW, Li L, Chen S, et al.** (2020) A plant-specific SWR1 chromatin-remodeling complex couples histone H2A.Z deposition with nucleosome sliding. *EMBO J* **39**: e102008.
- Manavella PA, Weigel D, Wu L** (2011) Argonaute10 as a miRNA locker. *Cell* **145**: 173–174.
- March-Diaz R, Reyes JC** (2009) The beauty of being a variant: H2A.Z and the SWR1 complex in plants. *Mol Plant* **2**: 565–577.
- Marques M, Laffamme L, Gervais AL, Gaudreau L** (2010) Reconciling the positive and negative roles of histone H2A.Z in gene transcription. *Epigenetics* **5**: 267–272.
- Meng X, Wang H, He Y, Liu Y, Walker JC, Torii KU, Zhang S** (2012) A MAPK cascade downstream of ERECTA receptor-like protein kinase regulates Arabidopsis inflorescence architecture by promoting localized cell proliferation. *Plant Cell* **24**: 4948–4960.
- Mizuguchi G, Shen X, Landry J, Wu WH, Sen S, Wu C** (2004) ATP-driven exchange of histone H2A.Z variant catalyzed by SWR1 chromatin remodeling complex. *Science* **303**: 343–348.
- Nadiya F, Anjali N, Thomas J, Gangaprasad A, Sabu KK** (2019) Deep sequencing identified potential miRNAs involved in defense response, stress and plant growth characteristics of wild genotypes of cardamom. *Plant Biol* **21**: 3–14.
- Nakagawa T, Suzuki T, Murata S, Nakamura S, Hino T, Maeo K, Tabata R, Kawai T, Tanaka K, Niwa Y, et al.** (2007) Improved Gateway binary vectors: high-performance vectors for creation of fusion constructs in transgenic analysis of plants. *Biosci Biotechnol Biochem* **71**: 2095–2100.
- Ojolo SP, Cao S, Priyadarshani S, Li W, Yan M, Aslam M, Zhao H, Qin Y** (2018) Regulation of plant growth and development: A review from a chromatin remodeling perspective. *Front Plant Sci* **9**: 1232.
- Olmedo-Monfil V, Duran-Figueroa N, Arteaga-Vazquez M, Demesa-Arevalo E, Autran D, Grimanelli D, Slotkin RK, Martienssen RA, Vielle-Calzada JP** (2010) Control of female gamete formation by a small RNA pathway in Arabidopsis. *Nature* **464**: 628–632.
- Pagnussat GC, Alandete-Saez M, Bowman JL, Sundaresan V** (2009) Auxin-dependent patterning and gamete specification in the Arabidopsis female gametophyte. *Science* **324**: 1684–1689.
- Parenicova L, de Folter S, Kieffer M, Horner DS, Favalli C, Busscher J, Cook HE, Ingram RM, Kater MM, Davies B, et al.** (2003) Molecular and phylogenetic analyses of the complete MADS-box transcription factor family in Arabidopsis: new openings to the MADS world. *Plant Cell* **15**: 1538–1551.
- Petesht SJ, Lis JT** (2008) Rapid, transcription-independent loss of nucleosomes over a large chromatin domain at Hsp70 loci. *Cell* **134**: 74–84.
- Pillitteri LJ, Torii KU** (2012) Mechanisms of stomatal development. *Annu Rev Plant Biol* **63**: 591–614.
- Pillitteri LJ, Bemis SM, Shpak ED, Torii KU** (2007) Haploinsufficiency after successive loss of signaling reveals a role for ERECTA-family genes in Arabidopsis ovule development. *Development* **134**: 3099–3109.
- Potok ME, Wang Y, Xu L, Zhong Z, Liu W, Feng S, Naranbaatar B, Rayatpisheh S, Wang Z, Wohlschlegel JA, et al.** (2019) Arabidopsis SWR1-associated protein methyl-CpG-binding domain 9 is required for histone H2A.Z deposition. *Nat Commun* **10**: 3352.
- Qin Y, Zhao L, Skaggs MI, Andreuzza S, Tsukamoto T, Panoli A, Wallace KN, Smith S, Siddiqi I, Yang Z, et al.** (2014) ACTIN-RELATED PROTEIN6 regulates female meiosis by modulating meiotic gene expression in Arabidopsis. *Plant Cell* **26**: 1612–1628.

- Qu LJ, Li L, Lan Z, Dresselhaus T** (2015) Peptide signalling during the pollen tube journey and double fertilization. *J Exp Bot* **66**: 5139–5150.
- Rabiger DS, Drews GN** (2013) MYB64 and MYB119 are required for cellularization and differentiation during female gametogenesis in *Arabidopsis thaliana*. *PLoS Genet* **9**: e1003783.
- Reiser L, Modrusan Z, Margossian L, Samach A, Ohad N, Haughn GW, Fischer RL** (1995) The BELL1 gene encodes a homeodomain protein involved in pattern formation in the *Arabidopsis* ovule primordium. *Cell* **83**: 735–742.
- Robinson-Beers K, Pruitt RE, Gasser CS** (1992) Ovule development in wild-type *Arabidopsis* and two female-sterile mutants. *Plant Cell* **4**: 1237–1249.
- Roe JL, Nemhauser JL, Zambryski PC** (1997) TOUSLED participates in apical tissue formation during gynoecium development in *Arabidopsis*. *Plant Cell* **9**: 335–353.
- Rosa M, Von Harder M, Cigliano RA, Schlogelhofer P, Mittelsten Scheid O** (2013) The *Arabidopsis* SWR1 chromatin-remodeling complex is important for DNA repair, somatic recombination, and meiosis. *Plant Cell* **25**: 1990–2001.
- Schauer SE, Jacobsen SE, Meinke DW, Ray A** (2002) DICER-LIKE1: Blind men and elephants in *Arabidopsis* development. *Trends Plant Sci* **7**: 487–491.
- Schneitz K, Hulskamp M, Pruitt RE** (1995) Wild-type ovule development in *Arabidopsis thaliana*: a light microscope study of cleared whole-mount tissue. *Plant J* **7**: 731–749.
- Schneitz K, Baker SC, Gasser CS, Redweik A** (1998) Pattern formation and growth during floral organogenesis: HUELLENLOS and AINTEGUMENTA are required for the formation of the proximal region of the ovule primordium in *Arabidopsis thaliana*. *Development* **125**: 2555–2563.
- Shpak ED, McAbee JM, Pillitteri LJ, Torii KU** (2005) Stomatal patterning and differentiation by synergistic interactions of receptor kinases. *Science* **309**: 290–293.
- Sijacic P, Holder DH, Bajic M, Deal RB** (2019) Methyl-CpG-binding domain 9 (MBD9) is required for H2A.Z incorporation into chromatin at a subset of H2A.Z-enriched regions in the *Arabidopsis* genome. *PLoS Genet* **15**: e1008326.
- Skopelitis DS, Hill K, Klesen S, Marco CF, von Born P, Chitwood DH, Timmermans MCP** (2018) Gating of miRNA movement at defined cell-cell interfaces governs their impact as positional signals. *Nat Commun* **9**: 3107.
- Su Z, Wang N, Hou Z, Li B, Li D, Liu Y, Cai H, Qin Y, Chen X** (2020) Regulation of female germline specification via small RNA mobility in *Arabidopsis*. *Plant Cell* **32**: 2842–2854.
- Su Z, Zhao L, Zhao Y, Li S, Won S, Cai H, Wang L, Li Z, Chen P, Qin Y, Chen X** (2017) The THO complex non-cell-autonomously represses female germline specification through the TAS3-ARF3 module. *Curr Biol* **27**: 1597–1609 e1592.
- Tang WH, Zhang Y, Duvick J** (2012) The application of laser microdissection to profiling fungal pathogen gene expression in planta. *Methods Mol Biol* **835**: 219–236.
- Tsikou D, Yan Z, Holt DB, Abel NB, Reid DE, Madsen LH, Bhasin H, Sexauer M, Stougaard J, Markmann K** (2018) Systemic control of legume susceptibility to rhizobial infection by a mobile microRNA. *Science* **362**: 233–236.
- Uchida N, Lee JS, Horst RJ, Lai HH, Kajita R, Kakimoto T, Tasaka M, Torii KU** (2012) Regulation of inflorescence architecture by intertissue layer ligand-receptor communication between endodermis and phloem. *Proc Natl Acad Sci USA* **109**: 6337–6342.
- van Daal A, White EM, Elgin SC, Gorovsky MA** (1990) Conservation of intron position indicates separation of major and variant H2As is an early event in the evolution of eukaryotes. *J Mol Evol* **30**: 449–455.
- Villanueva JM, Broadhvest J, Hauser BA, Meister RJ, Schneitz K, Gasser CS** (1999) INNER NO OUTER regulates abaxial-adaxial patterning in *Arabidopsis* ovules. *Genes Dev* **13**: 3160–3169.
- Wang H, Ngwenyama N, Liu Y, Walker JC, Zhang S** (2007) Stomatal development and patterning are regulated by environmentally responsive mitogen-activated protein kinases in *Arabidopsis*. *Plant Cell* **19**: 63–73.
- Wang H, Liu Y, Bruffett K, Lee J, Hause G, Walker JC, Zhang S** (2008) Haplo-insufficiency of MPK3 in MPK6 mutant background uncovers a novel function of these two MAPKs in *Arabidopsis* ovule development. *Plant Cell* **20**: 602–613.
- Wang P, Du Y, Li Y, Ren D, Song CP** (2010) Hydrogen peroxide-mediated activation of MAP kinase 6 modulates nitric oxide biosynthesis and signal transduction in *Arabidopsis*. *Plant Cell* **22**: 2981–2998.
- Wu MF, Tian Q, Reed JW** (2006) *Arabidopsis* microRNA167 controls patterns of ARF6 and ARF8 expression, and regulates both female and male reproduction. *Development* **133**: 4211–4218.
- Xu M, Leichty AR, Hu T, Poethig RS** (2018) H2A.Z promotes the transcription of MIR156A and MIR156C in *Arabidopsis* by facilitating the deposition of H3K4me3. *Development* **145**.
- Yadegari R, Drews GN** (2004) Female gametophyte development. *Plant Cell* **16 Suppl**: S133–S141.
- Yang WC, Sundaresan V** (2000) Genetics of gametophyte biogenesis in *Arabidopsis*. *Curr Opin Plant Biol* **3**: 53–57.
- Yu Y, Ji L, Le BH, Zhai J, Chen J, Luscher E, Gao L, Liu C, Cao X, Mo B, et al.** (2017) ARGONAUTE10 promotes the degradation of miR165/6 through the SDN1 and SDN2 exonucleases in *Arabidopsis*. *PLoS Biol* **15**: e2001272.
- Zhang Y, Wang P, Shao W, Zhu JK, Dong J** (2015) The BASL polarity protein controls a MAPK signaling feedback loop in asymmetric cell division. *Dev Cell* **33**: 136–149.
- Zhao L, He J, Cai H, Lin H, Li Y, Liu R, Yang Z, Qin Y** (2014) Comparative expression profiling reveals gene functions in female meiosis and gametophyte development in *Arabidopsis*. *Plant J* **80**: 615–628.
- Zhao L, Cai H, Su Z, Wang L, Huang X, Zhang M, Chen P, Dai X, Zhao H, Palanivelu R, et al.** (2018) KLU suppresses megasporocyte cell fate through SWR1-mediated activation of WRKY28 expression in *Arabidopsis*. *Proc Natl Acad Sci USA* **115**: E526–E535.
- Zhou Y, Honda M, Zhu H, Zhang Z, Guo X, Li T, Li Z, Peng X, Nakajima K, Duan L, et al.** (2015) Spatiotemporal sequestration of miR165/166 by *Arabidopsis* Argonaute10 promotes shoot apical meristem maintenance. *Cell Rep* **10**: 1819–1827.
- Zhu H, Hu F, Wang R, Zhou X, Sze SH, Liou LW, Barefoot A, Dickman M, Zhang X** (2011) *Arabidopsis* Argonaute10 specifically sequesters miR166/165 to regulate shoot apical meristem development. *Cell* **145**: 242–256.